JCTC Journal of Chemical Theory and Computation

Article

pubs.acs.org/JCTC

Spin-Polarized Electron Transport Across Metal–Organic Molecules: A Density Functional Theory Approach

Alexei Bagrets*

Institute of Nanotechnology, Karlsruhe Institute of Technology, 76344 Eggenstein-Leopoldshafen, Germany, and Steinbuch Centre for Computing, Karlsruhe Institute of Technology, 76344 Eggenstein-Leopoldshafen, Germany

ABSTRACT: In the field of molecular spintronics, experimental techniques have achieved a stage where it is feasible to explore the interplay between quantum electron transport and magnetism at the single molecule level. An example is a spin-polarized STM, which can probe local electrical currents through organic molecules deposited on magnetic surfaces. The atomistic complexity of nanoscale systems calls for a *first-principles* description of spin-dependent transport phenomena, e.g., based on the nonequilibrium Green's function (NEGF) formalism merged with density functional theory (DFT). However, for the case of molecular junctions with transition metal electrodes, a computation of the underlying Kohn–Sham Hamiltonian can be a challenging problem: a simultaneous and accurate description of spin ordered magnetic surfaces together with the electronic structure of a molecule is required. In the present work, we provide a solution for this problem. We present an implementation, within a standard quantum chemistry package, of the NEGF formalism with an efficient approximation for the self-energy, which accounts *both* for absorbing boundary conditions *and* for exchange splitting of the energy bands in ferromagnetic electrodes. We demonstrate an ability to simulate a variety of magnetic configurations including nanoscale domain walls, which are realized when a molecule with few spin centers is brought in contact with differently magnetized reservoirs. The magnetoresistance effect arising on the molecular scale is discussed based on examples including Ni atomic-sized contact, electron transport across a prototypical molecular magnet (vanadium-benzene multidecker cluster), and tunneling through Co-phthalocyanine. Furthermore, we verify the stability of magnetically nontrivial solutions against electron correlations within the DFT+*U* approach.

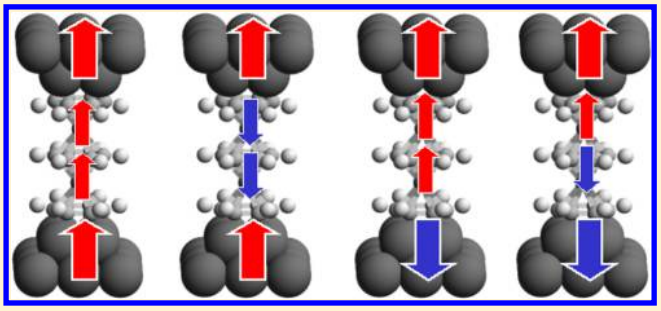

1. INTRODUCTION

The fastest ever passage, within only 10 years, had happened in the field of *spintronics* from the observation by Fert and Grünberg in 1988 of a giant magnetoresistance (GMR) effect in thin magnetic films[1,2] to its application in information technology. Nowadays, the intrinsic angular momentum of the electron—the spin—is employed together with electron charge for processing information in electronic devices. Moreover, advances in chemical synthesis and experimental techniques for a nanoscale manipulation triggered the imagination of researchers that conceptual ideas of *spintronics* can be merged with another branch of science, *molecular electronics*. That may result in nanoscale devices which exploit a functionality of molecules owing to both the charge and spin of the electron.

One example of such novel systems, being attractive for quantum computations, is a class of single molecule magnets where a coherent dynamics of spins has been already observed experimentally.[3] Another example is a family of metal-phthalocyanine (MePc) and metal-porphyrin molecules, which exhibit a propensity to switching phenomena[4] and spontaneous self-assembly.[5,6] These molecules combine delocalized π-electron clouds with the presence of transition-metal atoms whose spins can couple to a ferromagnetic substrate[7] and give rise to a formation of the hybrid spin-polarized states.[8−10] Observation of the spatial and energy structure of these interface states is possible with the help of spin-polarized STM.

Moreover, since in the experiments a measured tunneling current depends on the relative orientation of magnetizations of the tip and of the metallic surface, the spin-polarized STM is a natural tool to explore a concept of a molecular based spin-valve. Indeed, a dependence of the electron transport characteristics on magnetic configuration has been demonstrated recently: first, in the tunneling experiments through CoPc molecules,[11] and more recently in the GMR-type experiments,[12,13] where flexible H_2Pc molecules deposited on Co nanoislands or Mn-terminated films have been driven to establish a chemical bond to a ferromagnetic STM tip.

The delicate interplay of the electronic levels of a molecule and spin-ordering at the surface suggests the employment of density functional theory (DFT) methods to get insight into conduction mechanisms realized in particular experiments. Concerning quantum transport, one of the efficient approaches is based on the nonequilibrium Green's function (NEGF) formalism applied to Kohn–Sham (KS) particles.[14−17] Despite deficiencies of that "standard approach," which are mostly

Received: January 11, 2013
Published: April 29, 2013

   dx.doi.org/10.1021/ct4000263 | *J. Chem. Theory Comput.* 2013, 9, 2801−2815

related to the missing derivative discontinuity in the local (LDA) or semilocal (GGA) approximations to the exchange-correlation (xc) functionals,[18] the method—when focusing on qualitative aspects and trends—has proven to be a valuable tool in identifying many descriptors of transport experiments.[19−24] Furthermore, recent studies have provided encouraging evidence that, when combined with exact xc functionals for model systems, the KS conductance can reproduce the linear response of the interacting quantum dot systems[25] even in the Kondo regime (below the Kondo temperature) despite the absence of the Abrikosov−Suhl resonance in the KS spectral function.[26−28]

Suppose, we consider a two-terminal transport experiment where a molecule is brought into contact with two (ferromagnetic) electrodes, kept under different chemical potentials. Within the NEGF formalism, one looks upon this system as consisting of left (L) and right (R) hand side "reservoirs" coupled to an "extended molecule": this usually includes a molecule of interest but also a few tens of atoms of the nearby electrodes (see Figures 1a, 3a, 7b). Dynamics of electrons within the molecular subspace is described by the Green's function $G(E)$ satisfying the Dyson equation, $G^{-1}(E) = G_0{}^{-1}(E) - \Sigma_L(E) - \Sigma_R(E)$. It connects a propagator $G(E)$ of the coupled system to a propagator $G_0(E) = [E + i0 - H^{KS}]^{-1}$ of the isolated "extended molecule." The nonhermitian self-energies Σ_L and Σ_R account for the interaction with the reservoirs and together with G, via the NEGF formalism, define a particle density, which is to be found self-consistently (eq 3 in section 2.3). A nontrivial problem of finding self-energies can be resolved with the help of a recursive ("decimation") technique,[16,29] or circumvented with effective models, e.g., based on the Bethe lattice[30] or local-in-time (Markovian, energy-independent) approximation.[31,32]

Besides self-energies, another difficulty arises for nonperiodic spin-ordered systems, like molecular junctions with ferromagnetic electrodes. There, the energy landscape is complicated due to a large amount of competing low-energy magnetic excitations associated with transition metal atoms with partially filled d shells. As a result, finding an initial guess for a single-particle Hamiltonian H^{KS} of the "extended molecule" already poses a challenging problem for many standard electronic structure codes. Even more problematic is to approach different self-consistent solutions in the presence of open boundaries: not only a magnetically homogeneous solution is desired but also others like domain-wall configurations, where magnetizations in the electrodes are oriented antiparallel to each other. Furthermore, if an organic cage of a molecule hosts open-shell magnetic ions, molecular spins can be coupled via exchange interactions to magnetizations of the reservoirs: *a priory*, a variety of spin configurations may be expected, and unfavorable solutions should be ruled out based on energy considerations.

One option to cope with a part of the above problems is relying on the periodic boundary conditions within the "supercell" approach: this solution is provided, for example, by the SMEAGOL package.[16] In this setup, to exclude artificial interference effects ("cross-talks") between repeated images, a usage of quite large supercells is required,[33] which comes with computational costs. An alternative approach has been suggested recently by Heinze et al.,[34] where a supercell setup is avoided by using the representation of the Landauer conductance formula in terms of localized Wannier functions derived from the 1D full-potential augmented plane wave calculation. While the method shows the potential to study a spin-dependent electron transport in atomic contacts[34] and 1D wires,[35] applications to molecular junctions are yet to be demonstrated.

On the other hand, standard quantum chemistry codes, like TURBOMOLE,[36] avoid periodic calculations in **k**-space and operate with finite size clusters facing vacuum: there, an initial guess for the ground state wave function is usually given in terms of nonspin-polarized molecular orbitals based on the Hückel model. Since an energy profile for a cluster with tens of transition metal atoms has many local minima due to the presence of nearly degenerate spin multiplets, one may anticipate that desired magnetic solutions, which might parametrize H^{KS}, are almost impossible to achieve based on the Hückel guess only: this is fully confirmed by our experience where we typically end up with convergence problems.

To rationalize a problem, we show below how desired spin-ordered solutions can be obtained within the NEGF formalism implemented into a standard quantum chemistry code: namely, an iterative cycle has to be imposed on the trial density matrix subject to open spin-dependent boundary conditions. In brief, we adopt an energy-independent approximation for the self-energies $\Sigma_{L/R}$, which has been extensively tested in the earlier works,[31,32,37] also against experiments.[19,20] An imaginary piece of $\Sigma_{L/R}$ is responsible for electron absorption. Modification enters in a real piece of $\Sigma_{L/R}$, which acquires an additional term accounting for the exchange splitting of the energy bands in ferromagnetic electrodes [see section 2.2 for details]. As a result, at the boundaries to reservoirs, electrons feel "exchange" fields, which arrange their spins accordingly.

We have already applied successfully our formalism to rationalize STM-based spin-transport experiments across H_2Pc molecules.[12,13] Below, we provide details of the implementation and further show a potential of the method by examining magnetic and electron transport properties of a set of nanoscale systems, including Ni atomic-sized contact (section 3), small molecular magnets—vanadium−benzene mutidecker clusters (section 4), and CoPc molecules (section 5). Furthermore, we account for the Hubbard U term and discuss the stability of magnetic solutions against electron correlations [section 4.4, 4.5, and 5.2].

A formalism presented below is implemented by us into the original computer package AITRANSS (which stands for *ab initio* transport simulations).[38] It is interfaced to TURBOMOLE[36] and fully keeps its performance with regard to computation time and memory requirements, also at the computer workstation platforms. We stress, however, that conceptual ideas of the method are quite general. In particular, a pilot implementation linked to a massively parallel FHI-aims package[39] is currently under testing, with details to be presented in a forthcoming publication.

2. INTRODUCING MAGNETIC RESERVOIRS IN QUANTUM CHEMISTRY CALCULATIONS

2.1. Kohn−Sham Hamiltonian. A procedure to include magnetic reservoirs in quantum chemistry calculations is explained below on the example of Ni atomic-sized contacts. Experimentally, such nanoscale systems can be realized with STM[40] or the electromigrated break junctions technique.[41] We will closely follow the approach based on the concept of partitioning, as outlined in a previous work.[31] The contact region of the Ni atomic constriction is simulated on the atomistic level without a loss of accuracy and is referred as "extended molecule," $\mathcal{M}$ (see Figure 1a). It consists of two

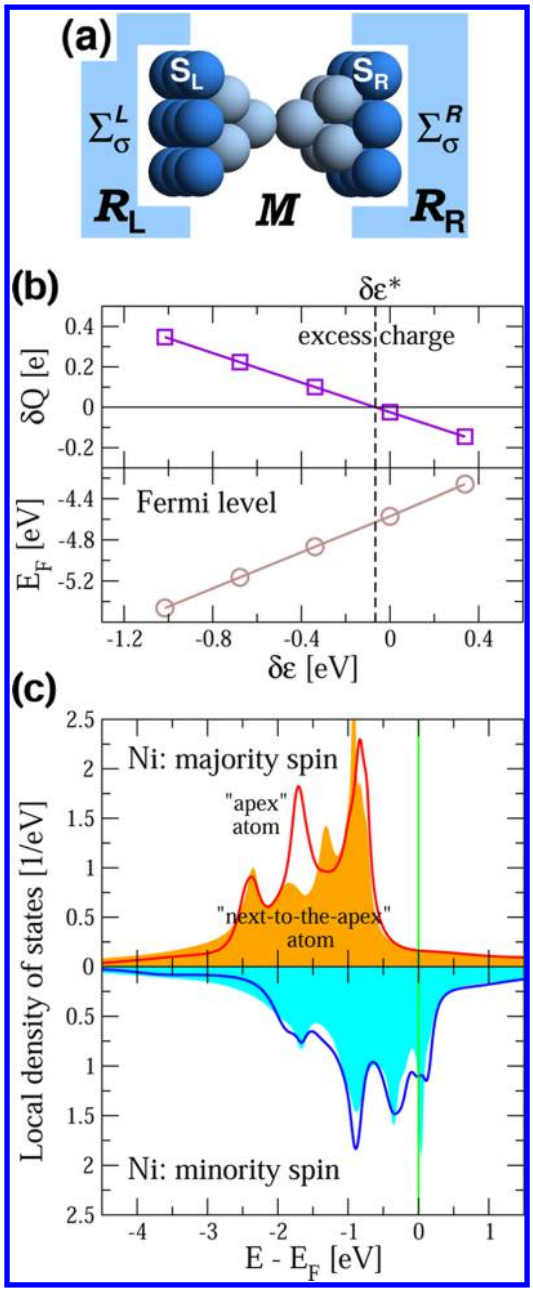

Figure 1. (a) Arrangements of atoms in Ni nanojunction. Its central region ("extended molecule," $\mathcal{M}$) consists of two pyramidal fcc(001) clusters joined via apex atoms and is described at the atomistic level. $\mathcal{M}$ is attached to the reservoirs, $\mathcal{R}_L$ and $\mathcal{R}_R$, representing left (L) and right (R) electrodes. Reservoirs are modeled by absorbing boundary conditions (see text for details), which are active at the outermost atomic planes, $\mathcal{S}_L$ and $\mathcal{S}_R$, of the simulation cluster $\mathcal{M}$. (b) Dependence of the excess charge, δQ, accumulated at the boundaries $\mathcal{S}_L$ or $\mathcal{S}_R$, and the dependence of the chemical potential, ε_F, on the energy shift $\delta\varepsilon$ parametrizing the self-energy. (c) Spin-polarized density of states at Ni atoms of the atomic constriction.

fcc(001) pyramidal clusters joined via apex atoms. The remaining degrees of freedom of the macroscopic system are referred as "reservoirs." In Figure 1a, reservoirs $\mathcal{R}_L$ and $\mathcal{R}_R$ are representing left (L) and right (R) hand side electrodes with spin-polarized electrons. An interaction between reservoirs and the atomistic subsystem $\mathcal{M}$ is accounted for by the model spin-dependent self-energies, Σ_L^σ and Σ_R^σ (here σ is a spin index), with details to be specified later.

The atomistic description is based on DFT as implemented in TURBOMOLE.[36] If not specified otherwise, calculations presented throughout the paper were carried out using a generalized gradient approximation (GGA, BP86 functional[42,43]), contracted Gaussian-type basis sets of split-valence quality with polarization functions (def-SVP),[44] and corresponding Coulomb-fitting basis sets[45] within the resolution of identity approximation.

As mentioned in the Introduction, our experience shows that a large amount of spin degrees of freedom introduces a convergence problem to a standard quantum chemistry calculation. Therefore, as the first step, we find the artificial closed-shell solution for the "extended molecule" M, representing (in the given example) a Ni cluster with 28 atoms and $N_{el} = 784$ electrons. Thus, we obtain a set of Kohn–Sham energies, ε_p^σ, and corresponding orbitals, $|p\sigma\rangle = \Sigma_\nu c_{p\nu}^\sigma |\nu\rangle$. They are expanded over nonorthogonal Gaussian-type basis functions $\langle \mathbf{x}|\nu\rangle = \varphi_\nu(\mathbf{x})$ with real-valued overlap integrals $S_{\nu\nu'} = \langle\nu|\nu'\rangle = \int d^3\,\mathbf{x}\,\varphi_\nu(\mathbf{x})\,\varphi_{\nu'}(\mathbf{x})$. Here and later, σ denotes a spin channel. For convenience, via the Löwdin orthogonalization procedure, the nonorthogonal basis can be transformed to the orthogonal one: $|\tilde{\nu}\rangle = \Sigma_{\nu'}|\nu'\rangle S_{\nu'\nu}^{-1/2}$. As for the latter, we assume all operators and corresponding matrices to be expressed in that orthogonal basis. The Kohn–Sham single-particle Hamiltonian can be reconstructed as $H^{KS} = \Sigma_\sigma H^\sigma$, where

$$H^\sigma = \sum_p |p\sigma\rangle \varepsilon_p^\sigma \langle p\sigma| = \sum_{\mu\nu} |\tilde{\mu}\rangle H_{\mu\nu}^\sigma \langle\tilde{\nu}| \quad (1)$$

with $H_{\mu\nu}^\sigma = \Sigma_{\mu'\nu'p} S_{\mu\mu'}^{1/2} c_{\mu'p}^\sigma \varepsilon_p^\sigma [c^\sigma]_{p\nu'}^T S_{\nu'\nu}^{1/2}$; here, the superscript T denotes a transpose matrix.

2.2. Approximation for the Self-Energy. *2.2.1. Preliminary Remarks.* When the "extended molecule" $\mathcal{M}$ is contacted to macroscopic leads, a propagation of the spin-σ electron with energy E within a subspace limited by $\mathcal{M}$ is described by Green's function $G^\sigma(E) = [E - H^\sigma - \Sigma^\sigma(E)]^{-1}$, where the self-energy $\Sigma^\sigma(E)$ accounts for the interaction between a finite system and reservoirs. A calculation of the exact self-energy is straightforward in principle but tedious in practice.[14,16] However, as has been argued in refs 31 and 32, if atomic clusters introduced to model parts of metallic electrodes include a sufficient number of atoms, results of transport calculations encoded in the transmission function become insensitive to the self-energy model used: in the limit of large atomic clusters, one approaches the exact solution. This statement has been illustrated in ref 32 where examples of the tight-binding 1D wire, Au atomic contact, and small organic molecule placed between Au leads have been discussed. In Appendix B, we present further examples in support of this idea and show results of benchmarking calculations of transport characteristics across a benzene-dithiol molecule, computed assuming different electrode sizes.

2.2.2. Spin-Dependent Boundary Conditions. More specifically, we adopt the approximation, where the reservoirs are modeled by modifying the spacial boundary conditions that the KS wave functions are subject to. In particular, we introduce absorbing boundary conditions,[31,32,46] which become active at the outermost atomic layers $\mathcal{S}_L$ and $\mathcal{S}_R$ of the tetragonal pyramids, representing parts of electrodes. In Figure 1a, these surface layers $\mathcal{S}_L$ and $\mathcal{S}_R$ are labeled by dark blue color. In the model, the spin-dependent ($\sigma = \pm 1$) self-energy $\Sigma^\sigma(E) \approx \Sigma_L^\sigma +$

Σ_R^σ is energy independent and is parametrized by the local function, which in the real-space representation is given by $\Sigma_{L/R}^\sigma(\mathbf{x},\mathbf{x}') = \langle \mathbf{x}|\Sigma_{L/R}^\sigma|\mathbf{x}'\rangle = [\delta\varepsilon(\mathbf{x}) + (\sigma/2)\Delta_{ex}^{L/R}(\mathbf{x}) - i\eta(\mathbf{x})] \times \delta(\mathbf{x} - \mathbf{x}')$. Here, local absorption rate $\eta(\mathbf{x})$, exchange fields $\Delta_{ex}^{L/R}(\mathbf{x})$, and corresponding compensating energy shift $\delta\varepsilon(\mathbf{x})$ are taking nonzero values at the surface regions $\mathcal{S}_L$ and $\mathcal{S}_R$ only. Possible choices for $\delta\varepsilon(\mathbf{x})$ and $\eta(\mathbf{x})$ are given in Appendix B. Below, we are assuming homogeneous functions, so the self-energy takes a form of the diagonal matrix:

$$\Sigma_{L/R}^\sigma = \sum_{\mu\nu\in S_{L/R}} |\tilde{\mu}\rangle\left[\delta\varepsilon + \frac{\sigma}{2}\Delta_{ex}^{L/R} - i\eta\right]\delta_{\mu\nu}\langle\tilde{\nu}| \quad (2)$$

Here, the absorption rate η is a parameter: following our previous experience, in the examples considered below, η = 0.05 Ha = 1.36 eV has been chosen such that the computed results for physical observables, like local densities of sates or ballistic transmission function, are almost independent under moderate variations of η. As specified in detail later, for the given value η of level broadening, the corresponding energy shift $\delta\varepsilon$ is adjusted by imposing the charge neutrality condition within the "extended molecule."

In eq 2, the term $(\sigma/2)\Delta_{ex}^{L/R}$ (with $\sigma = \pm 1$) accounts for the exchange splitting of the energy bands in ferromagnetic electrodes. In the case of Ni, a value $|\Delta_{ex}^{L/R}|$ = 0.6 eV has been used, which is characteristic for the d band and should be taken from independent first-principles calculation (see, e.g., ref 47). The additive term $(\sigma/2)\Delta_{ex}^{L/R}$ is acting at the interface regions $\mathcal{S}_L$ and $\mathcal{S}_R$ only. Its role should be understood as to modify the diagonal matrix elements of the KS Hamiltonian by introducing the energy splitting between up-spin and down-spin atomic levels and to sustain a source of the exchange field that polarizes electrons. Furthermore, we have ascertained that a combination of the chosen values for η and $\Delta_{ex}^{L/R}$ results in averaged magnetic moments of $\approx$0.6 μ_B at the interfaces $\mathcal{S}_L$ and $\mathcal{S}_R$, in agreement with bulk magnetic moment of Ni.

2.3. Density Matrix. Freedom to choose a sign of $\Delta_{ex}^{L/R}$ independently for the left (L) and right (R) reservoirs allows us, via the iterative procedure, to achieve different solutions corresponding either to parallel (P) or antiparallel (AP) alignment of magnetizations in the electrodes. Namely, according to the NEGF formalism, in the presence of open boundaries the particle density for spin-σ electrons in the subsystem $\mathcal{M}$ is defined via the density matrix $n^\sigma(\mathbf{x},\mathbf{x}') = \langle \mathbf{x}|D^\sigma|\mathbf{x}'\rangle = \Sigma_{\mu\mu'\nu\nu'}\varphi_\mu(\mathbf{x})\ S_{\mu\mu'}^{-1/2}D_{\mu'\nu'}^\sigma\ S_{\nu'\nu}^{-1/2}\varphi_\nu(\mathbf{x}')$, where

$$D^\sigma = \int_{-\infty}^{+\infty}\frac{dE}{2\pi}G^\sigma(E)[\Gamma_L^\sigma f(E-\mu_L) + \Gamma_R^\sigma f(E-\mu_R)] \times G^{\sigma\dagger}(E) \quad (3)$$

Here, $G^\sigma(E) = [E - H^\sigma - \Sigma_L^\sigma - \Sigma_R^\sigma]^{-1}$, with H^σ and $\Sigma_{L/R}^\sigma$ defined in eqs 1 and 2, $\Gamma_{L/R}^\sigma = i(\Sigma_{L/R}^{\sigma\dagger} - \Sigma_{L/R}^\sigma)$ are independent of energy, and $f(E-\mu_{L/R})$ are Fermi–Dirac distributions with corresponding chemical potentials $\mu_{L/R}$ in the reservoirs. Although a finite difference $\mu_L - \mu_R = eV$ allows us to simulate a response on the applied bias voltage V, in the following we assume a limit of zero bias and $\mu_L = \mu_R = \varepsilon_F$. A dramatic advantage of the Markovian (energy-independent) approximation for the self-energy is that the spectral integral in eq 3 can be performed analytically;[31] details are given in Appendix A.

Equipped with eq 3, at the second step of our calculation, we follow the modified iterative scheme which is controlled by the shell script. Given a guess for the Kohn–Sham wave functions, the density matrix is computed by the independent AITRANSS module according to eq 3. Next, the density matrix is admixed with that from the previous iteration, and the result is returned to TURBOMOLE to find a modified set of Kohn–Sham orbitals. The cycle is repeated unless the self-consistent solution, reflecting the spin-polarized electronic structure of the system, is reached.

2.4. Parametrized Self-energy Function and Charge Neutrality Condition. Since we do not perform a quantum chemistry (DFT) calculation for the magnetic bulk crystal with spin-polarized electrons, such as Ni, the Fermi energy ε_F is not known *a priori*. In our calculations, ε_F follows from its definition through the self-consistent procedure. More specifically, an initial guess for the Fermi energy, ε_F, is given by the closed-shell solution. We assume that our "extended molecule" is large enough so that all screening effects are taking place within the atomistic subspace $\mathcal{M}$. Due to a parametric dependence of the density operators $D^\sigma(\delta\varepsilon)$ on the energy shift $\delta\varepsilon$ entering the self-energies, eq 2, we adjust $\delta\varepsilon_n$ at each iteration n in such a way that the amount of electrons $\Sigma_\sigma Tr\, D^\sigma(\delta\varepsilon_n) = N_{el}$ is fixed to satisfy the charge neutrality condition within $\mathcal{M}$ under given ε_F. After iterations are converged, we get $\delta\varepsilon = \delta\varepsilon_\infty$. Next, we perform few additional self-consistent calculations assuming slightly different estimates for the Fermi energy ε_F in the reservoirs. The associated energy shift $\delta\varepsilon$ is found to be almost a linear function on the Fermi energy guess ε_F, see Figure 1b, lower plot.

To proceed further, for every self-consistent calculation with given ε_F and associated energy shift $\delta\varepsilon$, we compute the excess (Löwdin) charge accumulated at the interface atomic plane $\mathcal{S}_L$ or $\mathcal{S}_R$: $\delta Q = (\sum_{\sigma,\mu\in S_{L/R}} D_{\mu\mu}^\sigma) - Q^{ref}$, where Q^{ref} = 28·9 = 252 electrons in the considered example. We consider δQ as a function of $\delta\varepsilon$: the result is shown in Figure 1b, upper plot. Even though δQ is less that 0.5e per nine atoms, in general $\delta Q(\delta\varepsilon) \neq 0$ for arbitrary $\delta\varepsilon$. We argue that for the given number of atoms in the electrode, the best parametrization of the model self-energy, eq 2, is achieved with such a parameter $\delta\varepsilon^*$, when the electron charge at the interface between atomistic subsystem $\mathcal{M}$ and the reservoir $\mathcal{R}_R$ or $\mathcal{R}_L$ is approaching the bulk value, i.e., $\delta Q(\delta\varepsilon^*) = 0$ (Figure 1b, upper plot). The energy shift $\delta\varepsilon^*$ and corresponding Fermi level $\varepsilon_F(\delta\varepsilon^*)$ are used later on in transport calculations.

In the considered example of Ni nanojunction, we have obtained ε_F = −4.63 eV, which is underestimated as compared to experimentally measured values, 5.05–5.35 eV, of the Ni work function.[48] We attribute the difference to the finite size effects: the amount of atoms in our clusters is quite small as compared to the thermodynamic limit. We note, however, that the inaccuracy in the Fermi level determination can be partially eliminated when plotting results for $T(E)$ with respect to ε_F (see example in Appendix B).

3. APPLICATION TO NI ATOMIC CONTACT

We first consider Ni atomic contact (Figure 1a) and the case of parallel alignment of magnetizations in the reservoirs. We plot in Figure 1c the atom (A) projected (or local) density of states, $\rho_A^\sigma(E) = -(1/\pi)\Sigma_{\mu\in A} Im\ G_{\mu\mu}^\sigma(E)$, at the apex and the next-to-the-apex atoms. We observe that within the outlined approach a desired mean-field type solution describing ferromagnetic spin ordering in the Ni atomic contact is indeed achieved. Namely, the density of states at Ni atoms is spin-polarized, with the majority spin band being almost occupied and the minority spin

band crossing the Fermi level (Figure 1c). On the basis of the Löwdin population analysis, we found a magnetic moment of 0.61 μ_B at the next-to-the-apex atom. Due to the reduced coordination number, a slightly larger moment of 0.66 μ_B is found at the apex atom (see Figure 2, solid line).

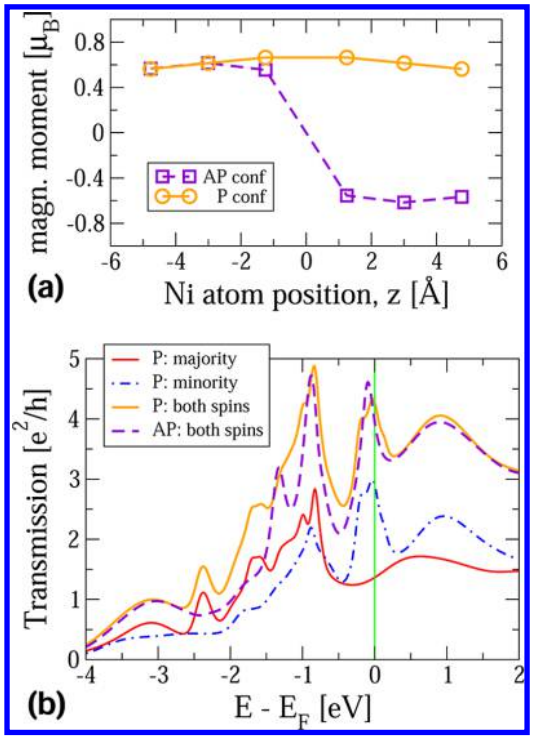

Figure 2. Upper plot (a): computed magnetic moments at Ni atoms of the atomic-sized constriction shown in Figure 1a. In the case of parallel (P) alignment of magnetizations in the electrodes, the magnetization profile is homogeneous: solid line with open circles. In the case of antiparallel (AP) alignment of magnetizations, an abrupt atomic-scale domain wall is pinned to the atomic constriction: dotted line with open squares. Lower plot (b): associated energy-dependent transmission functions. Dashed magenta line, AP alignment with the domain wall; solid orange line, P alignment. For the case of P alignment, transmission is decomposed to the majority spin (red solid thin line) and minority spin (blue dashed-dotted thin line) channels.

Furthermore, assuming the sign of $\Delta_{ex}^{L/R}$ in the self-energy parametrization (eq 2) to be different in the opposite reservoirs (the case of antiparallel alignment of magnetizations), we find a well converged collinear spin-ordered solution, which describes an atomically sharp domain wall. The magnetization profile across the domain wall is shown in Figure 2a (dotted line) with spins flipping at the apex atoms. Magnetic moments localized at these atoms, 0.55 μ_B, are a bit smaller as compared to 0.66 μ_B found for the case of homogeneous magnetization profile, reflecting the "softening" of the magnetic moment in the domain wall.[49] Results agree with our previous calculations performed by the KKR electronic structure method.[50] We emphasize that the structure of the domain wall is a result of the self-consistent calculation and is not imposed on purpose, except for boundary conditions.

Next, we consider the transmission function, $T^\sigma(E)$, which also probes the spin-polarized electronic structure of the Ni atomic contact. According to the Landauer formalism, conductance g of the quasi-one-dimensional system is related to transmission $T(E) = \Sigma_\sigma T^\sigma(E)$ taken at the Fermi energy, $g = (e^2/h)T(\varepsilon_F)$. At zero bias, transmission per spin channel σ is evaluated as $T^\sigma(E) = \mathrm{Tr}[\Gamma_L^\sigma G^\sigma(E)\Gamma_R^\sigma G^{\sigma\dagger}(E)]$. Our results are shown in Figure 2b. In agreement with earlier calculations,[50,51] we observe that in the case of a uniform magnetization across the junction (P configuration), transmissions in up-spin and down-spin channels are shifted along the energy axis by ~0.8 eV, reflecting the spin-splitting of the Ni d band (cf. Figure 1c). In the case of the abrupt domain wall (AP configuration), transmission of the junction is somewhat lower, $T_{AP}(E) \lesssim T_P(E)$, indicating slightly enhanced scattering of electrons. At the Fermi level, conductances g_P and g_{AP} are close to $\sim 4e^2/h$ with the relatively small magnetoresistance ratio,[50,52,53] MR = $(g_P - g_{AP})/g_{AP}$, on the order of ~10%.

We note that, as compared to atoms in the bulk, Ni atoms in the nanocontact have smaller coordination numbers and, therefore, may be subject to stronger electron correlation effects. In particular, a possibility of Kondo screening of the localized spins in nanocontacts below the Kondo temperature T_K has been discussed,[54,55] with T_K reaching values up to ~100K. Description of such correlation effects is beyond the scope of the local exchange-correlation functionals like the generalized gradient approximation (GGA) used in this work. Thus, results and discussion presented above should be understood is being limited to the "high" temperature range, $T > T_K$. A spurious self-interaction is another drawback of the (semi)local functionals. We mention at this point that one of the computationally cheapest ways to verify stability of the obtained solutions is based on the DFT+U approach, which will be discussed in the following section on the example of vanadium-benzene multidecker clusters.

We also mention that even though our discussion has been limited to collinear spin orientations, a noncollinear spin arrangement may be relevant for many electron transport experiments on the nanoscale. For example, the case of transition metal nanowires has been discussed in the literature, where the noncollinear spin arrangement may be energetically favorable as compared to collinearly aligned magnetic moments in the domain wall.[49,56] In this regard, any nanoscale system with frustrated bonds, or where frustration may be induced by the interaction with a magnetic substrate, could show noncollinear magnetic ordering. Examples are Mn impurities within Co magnetic contacts,[35] or "Dy_3" and "V_{15}" single molecule magnets.[57,58] A description of quantum transport across these atomic or molecular junctions could be possible provided the outlined formalism is reformulated in terms of two-component spinor representation, and DFT exchange-correlation functionals account for the spin noncollinearity.[59,60]

4. ELECTRON TRANSPORT ACROSS SMALL MOLECULAR MAGNETS

4.1. Geometry of Molecular Junction. In this section, we consider a methodological example of a molecular scale spin-valve shown in Figure 3a. We imagine a molecular junction comprising a small molecular magnet, $V_2(C_6H_6)_3$ sandwich-like cluster, which is coupled to ferromagnetic Ni electrodes. For a possible realization, we refer to soft-landing experiments with $V_n(C_6H_6)_{n+1}$[61,62] and $TbPc_2$ molecules,[63,64] and recent spin-polarized STM based measurements of the GMR signal across single phthalocyanines.[12,13] We therefore assume that one Ni electrode could be a tip of a spin-polarized STM, while the other Ni electrode could be a magnetic nanoisland deposited on the metallic substrate. Ni electrodes are modeled by small fcc(001) clusters, comprising 13 atoms each, as shown in

dx.doi.org/10.1021/ct4000263 | J. Chem. Theory Comput. 2013, 9, 2801−2815

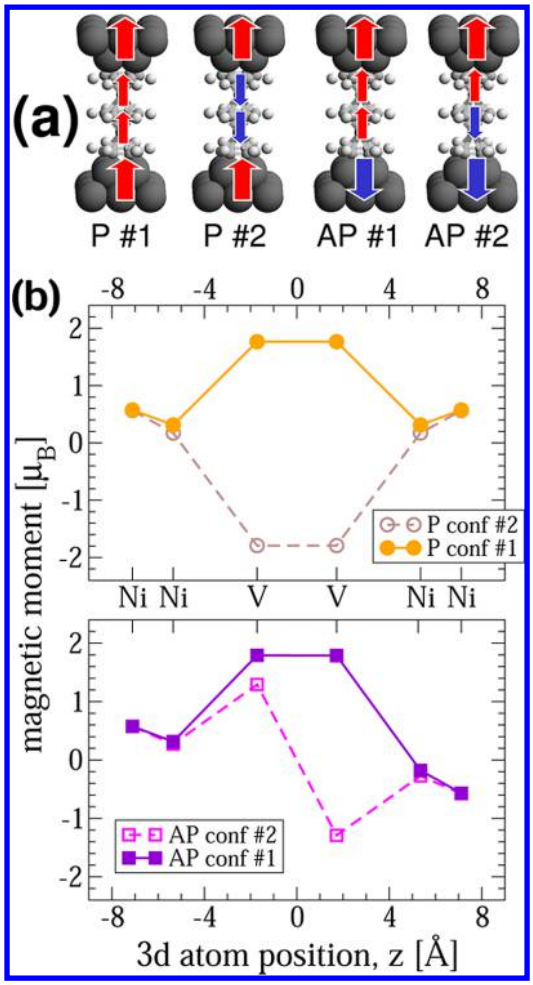

Figure 3. Upper plot (a): possible collinear alignments of magnetic moments in the molecular junction comprising the V_2Bz_3 cluster placed between magnetized Ni electrodes. Corresponding energies of magnetic configurations are listed in Table 1. Lower plot (b): calculated values of magnetic moments across junctions with either parallel or antiparallel aligned magnetizations of Ni electrodes.

Figure 3a. We also assume that frontier benzene rings of the molecules are placed on top of the hollow sites of the fcc(001) surfaces that corresponds to the energetically most favorable configuration.[65] Though the spin−orbit interaction is not accounted for in our calculations, Figure 3a implies that, due to a shape anisotropy, direction of magnetization in both magnetic electrodes would be perpendicular to the fcc (001) surface and would point along the z axis of the molecular magnet. In analogy with Co(111) nanoislands considered in the work by Schmaus et al.,[12] we assume that our bottom Ni cluster ("nanoisland") may have a magnetic moment pointing either parallel (P) or antiparallel (AP) with respect to the magnetization of the upper Ni cluster ("the STM tip").

The choice of V-Bz molecules (here and later, Bz refers to C_6H_6) is motivated by our earlier study. Namely, DFT calculations have shown that a hypothetical infinite V-Bz wire, which could be considered as a limiting case of the quasi-one-dimensional V_nBz_{n+1} clusters when $n \to \infty$, would sustain a fully spin-polarized current.[66,67] The "half-metal"-type band structure of infinite wire implies a metallic conductivity for the majority spin electrons but a semiconductor-like behavior for the minority spin electrons. One can therefore come to the intriguing conclusion that a short segment of the wire may act as a spin filter. Furthermore, both spin channels may be blocked in case the AP arrangement of magnetic moments is realized in the spin-valve junction. That could give rise to a large MR ratio, being of importance for applications in spintronics.

4.2. Electronic Structure of a Free V_2Bz_3 Cluster. Before discussing possible spin configurations realized in the molecular junction, we restate details of the electronic structure of the isolated clusters. In particular, earlier studies have shown that an infinite organometallic V-Bz wire would have an integer magnetic moment of 1 μ_B per unit cell, localized mainly on V atoms.[66] Once the spin−orbit interaction is switched on, magnetic moments are aligned along the wire axis.[68] We illustrate further inherent magnetic properties of the V_2Bz_3 cluster of our choice, by presenting its spin-polarized KS spectrum in Figure 4. There, we plot the spectral function

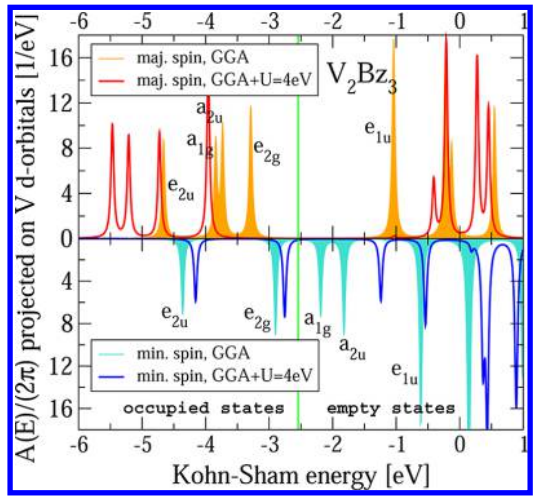

Figure 4. Kohn−Sham spectral function of a free V_2Bz_3 molecule projected on vanadium d orbitals (artificial level broadening η = 0.05 eV is implied) computed within the GGA and GGA+U (=4.0 eV) functionals.

projected on vanadium basis functions with d character. Our analysis shows that in the energy window from −5 eV up to −1.5 eV, all frontier molecular orbitals have significant admixture of vanadium d states.

For the charge neutral molecule, an open-shell solution could be envisaged from the odd number of d electrons associated with the isolated V atom, which has an $[Ar]3d^34s^2$ electronic configuration. In the molecule, a crystalline field splits V atomic levels. The s levels are pushed up in energy, so that five d electrons per each V atom are left over and need to be redistributed among the two spin channels. In particular, the pairs of d_{xy} and $d_{x^2-y^2}$ orbitals localized at two vanadium atoms are hybridized with π orbitals of benzene rings and form double degenerate states of e_{2u} and e_{2g} symmetry, which are double occupied in both spin channels, see Figure 4. (Here and later, we use common notations of the irreducible representations of the D_{6h} point symmetry group associated with V_2Bz_3 cluster). On the other hand, the d_{xz} and d_{yz} states contribute to the unoccupied degenerate e_{1u} molecular states. Next, the non-degenerate a_{1g} and a_{2u} states have mainly vanadium d_{z^2} character and are filled by up-spin electrons only. Therefore, the isolated molecule picks up a magnetic moment of 2 μ_B. In particular, (Löwdin) magnetic moments of $\simeq$1.2 μ_B are

dx.doi.org/10.1021/ct4000263 | J. Chem. Theory Comput. 2013, 9, 2801−2815

localized at two V atoms, while the small and negative moments are carried by C atoms.

4.3. Spin Configurations in Molecular Junction. *4.3.1. Solutions with Open Boundary Conditions.* When the V_2Bz_3 cluster is embedded into the nanogap between magnetic contacts, the V spins interact also with local magnetic moments of the Ni electrodes. Employing the NEGF formalism outlined in section 2, we have computed the electronic structure of molecular bridges, considering four possible magnetic configurations with collinear spin arrangements shown in Figure 3a. As it was described in detail in section 2, the P or AP alignment of magnetizations in the electrodes have been introduced via the spin-dependent boundary conditions encoded into the self-energies. Furthermore, at the initial steps of the DFT-NEGF iterative cycle, we fix orientations of spins localized at V atoms and at those Ni atoms, which are not at the immediate vicinity to reservoirs. For that, we introduce sources of the small local exchange fields, $\delta\Delta_{ex}^{V/Ni}$. Namely, diagonal matrix elements of the Hamiltonian associated with basis functions of V or Ni atoms acquire corresponding corrections $\delta h_{\mu\nu}^{\sigma} = \pm(\sigma/2)(\delta\Delta_{ex}^{V/Ni})\delta_{\mu\nu}$ (here $\sigma = \pm 1$ is a spin index), so that resulted spin densities projected at V and Ni atoms are becoming polarized. When the density matrix is iterated, corrections $\delta h_{\mu\nu}^{\sigma}$ to the Hamiltonian are switched off as soon as V and Ni atoms acquire spin magnetic moments aligned in the desired direction. Thus, multiple solutions can be found: corresponding magnetizations profiles are presented in Figure 3b.

4.3.2. Solutions with Free Boundary Conditions. A given magnetic configuration will have feedback on the conductance of the molecular junction. To discriminate the most favorable solutions, we have computed relative energies of different spin configurations of the molecular bridges. To avoid a possible dependence of the energy on the parameters entering the self-energy function, we have restricted ourselves to the calculation of energies of the isolated $Ni_{13}-V_2Bz_3-Ni_{13}$ clusters facing vacuum (Figure 3a). Here we imply that good estimates of the relative energies associated with rotations of spins can be obtained without taking into account open boundary conditions.

To obtain different magnetic solutions for isolated clusters, the AITRANSS module is switched to iterate the equilibrium density matrix of the closed system. To construct an initial guess for the spin-polarized density reflecting desired magnetic solution, we proceed as follows. Given the KS Hamiltonian $H_{\mu\nu}^{0}$ of the closed shell solution (here and later, the orthogonalized basis is assumed), we first split, via artificially introduced local exchange fields, diagonal matrix elements of $H_{\mu\nu}^{0}$ associated with basis functions of V or Ni atoms, $\tilde{H}_{\mu\nu}^{\sigma} = H_{\mu\nu}^{0} \pm(\sigma/2)\delta\Delta_{ex}^{V/Ni}\delta_{\mu\nu}$. Here the $(\pm)$-signs reflect desired orientation of the local magnetic moments. Next, we solve the eigenvalue problem for the trial Hamiltonian, $\Sigma_\nu \tilde{H}_{\mu\nu}^{\sigma}\tilde{c}_{\nu p}^{\sigma} = \tilde{c}_{\mu p}^{\sigma}\tilde{e}_{p}^{\sigma}$, and construct the initial guess for the spin-polarized density matrix as $\tilde{D}_{\mu\nu}^{\sigma} = \Sigma_p^{occ}\tilde{c}_{\mu p}^{\sigma}[\tilde{c}^{T}]_{p\nu}^{\sigma}$ (here, summation is limited to occupied electronic states). This trial density matrix is passed to TURBOMOLE to solve the KS equations. The resulted KS wave functions are used by AITRANSS to construct the updated density matrix (of the closed system). A small parameter, on the order of 1%, is used to admix the density matrices to ensure that the desired (initial) orientations of magnetic moments are not destroyed. The cycle is repeated unless the self-consistent solution is found, with energy being converged up to 10^{-5} eV.

We have observed that, as compared to the NEGF solution (Figure 3b) with the density matrix computed according to eq 3, magnetic moments at Ni atoms of the isolated $Ni_{13}-V_2Bz_3-Ni_{13}$ clusters are increased by a factor ~1.75, while the moments at V atoms are not affected by modified boundary conditions. However, we have found that in the molecular junction, as compared to a free V_2Bz_3 molecule, local magnetic moments at V atoms are slightly increased, up to $\approx 1.8\ \mu_B$.

4.3.3. Discussion of Results. Relative energies of four magnetic configurations (Figure 3a) are listed in Table 1

Table 1. Relative Energies of Magnetic Configurations Realized in $Ni_{13}-V_2Bz_3-Ni_{13}$ Clusters Shown in Figure 3a[a]

	relative energy [eV]	
configuration	this work	FHI-aims
P conf. #1	0.000	0.000
P conf. #2	0.320	0.212
AP conf. #1	0.104	0.089
AP conf. #2	0.398	0.476

[a]Results given in the second column ("this work") are obtained with def-SVP Gaussian basis set[44,45] from the TURBOMOLE[36] library and BP86[42,43] functional. Results given in the third column are obtained employing FHI-aims package[39] with "tight" (tier2) numerical basis set, PBE functional[69] and perturbative scalar relativistic corrections.

(second column). The P configuration #1 with all spins pointing up (Figure 3, solid line with circles) has the lowest energy. The P configuration #2 corresponds to the entire magnetic moment of V_2Bz_3 cluster being flipped with respect to Ni magnetizations (Figure 3, dotted line with circles): this configuration is higher in energy by 0.320 eV. Such a barrier implies that a rotation of the magnetic moment associated with the molecule would be stable against thermal fluctuations (kT = 0.025 eV). A creation of only one atomic scale "domain wall" at the interface between the V_2Bz_3 cluster and one of the Ni electrodes costs a factor ~2 smaller energy, namely 0.104 eV (AP configuration #1, Figure 3, solid line with squares). In contrast, the AP configuration #2 with antiferromagnetically arranged V spins within the molecule (Figure 3, dotted line with circles) is higher in energy by 0.398 eV and thus is very unlikely.

Our experience shows that obtaining desired and converged solutions describing different magnetic configurations can be quite a challenging task. To supplement our findings, we have also performed calculations of the ground state energies of the isolated $Ni_{13}-V_2Bz_3-Ni_{13}$ clusters using the FHI-aims computer package.[39] The FHI-aims is an all-electron electronic structure code, which employs a basis set of the numerically tabulated atom-centered orbitals. It allows one to prepare trial charge and spin density from the superposition of free-atom densities, taking into account an initial guess for the local spin moments at open-shell atoms. Computed DFT energies (within the PBE functional,[69] FHI-aims "tier2" basis set, and the scalar relativistic approximation) are listed in Table 1, third column: they compare well with results obtained using the Gaussian basis sets from the TURBOMOLE library (second column). Small changes can be attributed to scalar relativistic corrections and different, analytical vs numerical, basis sets used.

4.4. Account for Electron Correlations within DFT+*U* Approach. Electron transport across molecules is susceptible to the mutual alignment of the molecule's and electrodes'

dx.doi.org/10.1021/ct4000263 | J. Chem. Theory Comput. 2013, 9, 2801−2815

electronic levels and related to that partial charge transfer.[18,70−72] Because of the spurious self-interaction and missing derivative discontinuity inherent to the local or quasi-local functionals (like GGA BP86 used in this work), a description of the relative positions, with regard to the Fermi level, of the molecular resonances associated with localized d electrons can be particularly problematic in our case. To have a better control over the situation, we shall follow a computationally cheap procedure, namely the DFT+U (or more commonly, the LDA/GGA+U) approach.[73] In a nutshell, the DFT+U provides a simple form of the orbital dependent functional[74] which treats localized d (or f) electrons on the Hartree−Fock level, thus correcting for the spurious self-interaction.

Since the DFT+U is not available in TURBOMOLE, we have implemented it into our transport simulation package AITRANSS; details are given in Appendix C. To illustrate the implementation, in Figure 4 we first compare KS spectral functions, projected on d orbitals, of the free V_2Bz_3 cluster computed with the GGA BP86-functional[42,43] and with the (self-consistent) GGA+U approach, where GGA has been corrected by the U = 4.0 eV term switched on at the two V atoms. An open shell solution with two unpaired electrons is preserved. In essence, we observe a flow of the electronic spectrum as a function of the Coulomb repulsion U: unoccupied d-like orbitals are pushed up in energy while most of the occupied d-like orbitals are pushed down. The orbital energy shifts depend on the fractional contributions, associated with d electrons, to the levels' occupation numbers: the more d character is attributed to the given molecular orbital, the larger its energy shift is. For example, the up-spin e_{2g} HOMO doublet is shifted down by ≃1.5 eV, while the energy of empty up-spin e_{1u} states is raised by ≃1.75 eV. Similarly, the down-spin LUMO a_{1g} level is shifted upward by ≃2 eV. In contrast, the orbital energy of the down-spin e_{2g} HOMO doublet is only slightly affected by U, since these are hybrid molecular states with a substantial contribution from the benzene π orbitals.

4.5. Spin-Filtering and MR Effects. Equipped with DFT+U, we proceed now with a discussion of electron transport properties of Ni−V_2Bz_3−Ni junctions. In Figure 5, left column, we show spin-resolved transmission functions $T_P^\sigma(E)$ computed for the uniformly magnetized system with the lowest energy (P conf. #1, see Figure 3a and Table 1). In the case of U = 0 eV (upper left plot, pure GGA functional), conductance ∼0.75e^2/h is dominated by minority spin electrons, while the quasi-gap of ∼1.5 eV is found in the majority spin transmission. This result could be anticipated already from the KS spectrum of the system (Figure 4), which shows quite different HOMO−LUMO gaps in the up-spin and down-spin channels. Spin polarization of the current $P_I = [T_P^\uparrow(E_F) - T_P^\downarrow(E_F)]/T_P^\uparrow(E_F)$ is close to 90%, displaying a spin-filtering effect in agreement with our earlier results.[66] Furthermore, the effect is stable when Hubbard U term is switched on. Indeed, we see that for the larger U values (2.0 and 4.0 eV) minority spin transmission at E_F is reduced, but at the same time the quasi-gap in the up-spin channel further opens up. Current spin polarization P_I increases and approaches 99% at U = 4 eV.

Whether or not a significant spin polarization of the current could be converted to the large MR signal can be judged from Figure 5, right column. There, we compare transmission across the molecular junction with the parallel (P conf. #1, Figure 5) and antiparallel (AP conf. #1, Figure 3) orientation of magnetizations in Ni electrodes. The chosen AP configuration

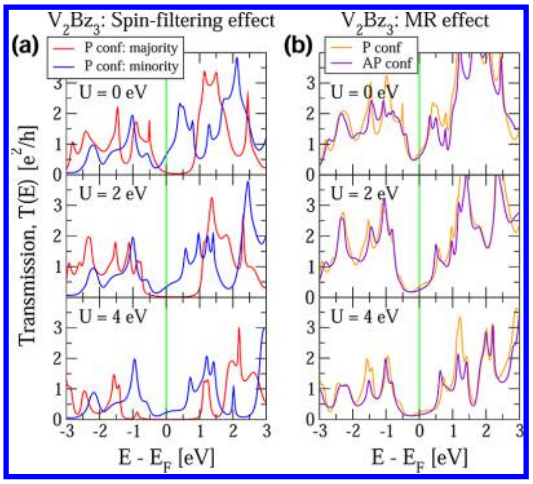

Figure 5. Left plot (a): spin-resolved transmission functions across Ni−V_2Bz_3−Ni junction with a parallel alignment of magnetizations in Ni electrodes (P conf.#1 at Figure 3a). Right plot (b): energy dependent transmission functions across Ni−V_2Bz_3−Ni junctions with either parallel (P conf.#1 at Figure 3a) or antiparallel (AP conf.#1 at Figure 3a) aligned magnetizations in electrodes. Plots highlight a flow of results as function of Coulomb repulsion U among d electrons of V atoms.

#1 has significantly smaller energy, as compared to the AP conf. #2, and does not affect a local magnetic moment of the V_2Bz_3 cluster. However, similar to the Ni atomic junction, an atomically sharp "domain wall" reduces the AP transmission as compared to the P one, also at the Fermi level: $T_{AP}(E_F) < T_P(E_F)$. The increase of the current spin-polarization P_I at larger U is followed by the increase of MR ratio, which is defined as MR = $[T_P(E_F) - T_{AP}(E_F)]/T_{AP}(E_F)$. The MR ratio raises from 23% at U = 0 eV, over 45% at U = 2 eV, and up to 58% at U = 4 eV.

To clarify details of the conduction mechanism, we present in Figure 6 the spin resolved local density of states (LDOS) at the V_2Bz_3 cluster within the junction, as well as a decomposition of the LDOS into "coupled molecular states" $|M,\sigma\rangle$ of V_2Bz_3. More specifically, we define $|M,\sigma\rangle$ (with σ being a spin index) as eigenstates of the hermitian block $P_\mathcal{M}H^\sigma P_\mathcal{M}$ of the KS-Hamiltonian H^σ (eq 1) associated with the Hilbert subspace $\mathcal{M}$ of the molecule. Here, $P_\mathcal{M} = \sum_{\mu\in\mathcal{M}} |\tilde{\mu}\rangle\langle\tilde{\mu}|$ is the orthogonal projector on $\mathcal{M}$ defined via orthogonalized basis functions originating from atoms of the molecule. In case of weak coupling to electrodes, the eigenstates $|M,\sigma\rangle$ closely resemble molecular orbitals in vacuum, while in general case effects of hybridization to the leads are taken into account. Since eigenstates $|M,\sigma\rangle$ form a complete basis in $\mathcal{M}$, the LDOS at the molecule can be viewed as a sum of individual contributions, $\rho_\mathcal{M}^\sigma(E) = -\frac{1}{\pi}\sum_M \langle M,\sigma|\mathrm{Im}\, G^\sigma(E)|M,\sigma\rangle$.

In Figure 6, we show such contributions to the LDOS originating from frontier molecular states of the V_2Bz_3 cluster, which arise in part from bonding and antibonding combinations of vanadium orbitals with d character. We see that in both spin channels some states, namely the ones with d_{z^2} symmetry (formerly a_{1g} and a_{1u} states) and with d_{xz} and d_{yz} symmetry (formerly e_{1u} states, cf. Figure 4) show up as well pronounced resonances. They are placed either well below (−2...−3 eV) or above (+0.5...+1.75 eV) the Fermi level, with exact energies being Hubbard U dependent. These resonance states are not responsible for conductance therefore. On the other hand,

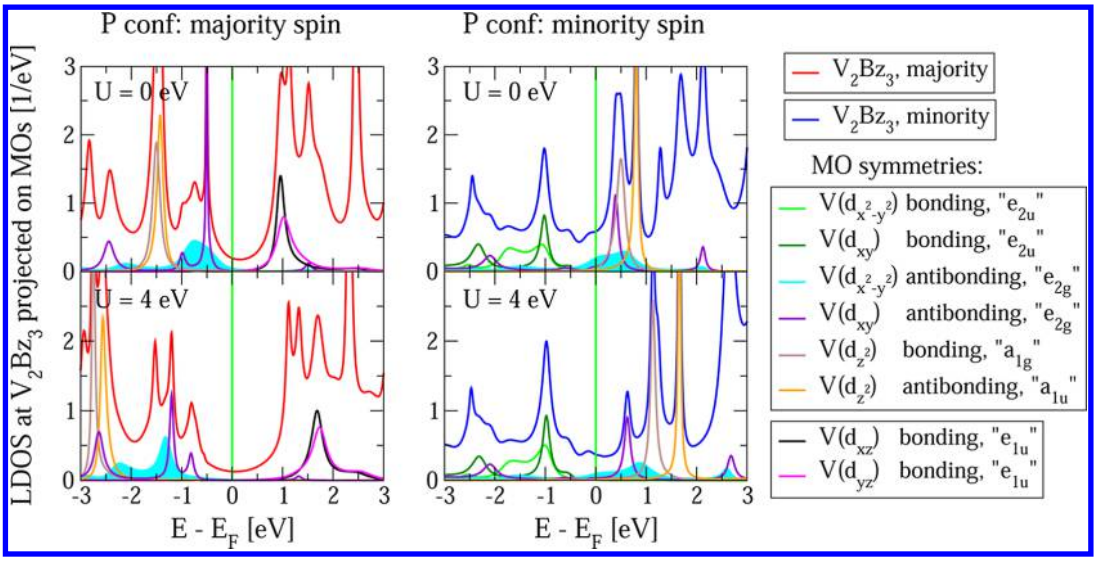

Figure 6. Spin resolved local density of states (LDoS) at V_2Bz_3 placed between Ni electrodes with parallel aligned magnetizations, and decomposition of LDoS into contributions associated with frontier molecular orbitals (MOs) of the V_2Bz_3 cluster (cf. Figure 4).

molecular orbitals with $d_{x^2-y^2}$ and d_{xy} symmetry (formerly e_{2u} and e_{2g} states) are strongly hybridized with electronic states in Ni electrodes and exhibit much broader structures (quasi-bands) in the local density of states. In particular, in the minority spin channel, the LDOS at E_F and, consequently, conductance are dominated by the contributions originating from e_{2g} down-spin LUMO doublet (cf. Figure 4). In contrast, in the majority spin channel, the e_{2g} HOMO derived states are almost occupied and provide only marginal contribution to conduction. Thus, the electron current is strongly spin polarized. A leakage of charge from minority LUMO states furthermore supports larger local magnetic moments found at vanadium atoms in the junction (1.8 μ_B as compared to 1.2 μ_B for a free cluster). Note that our results remain also valid when Hubbard U term is switched on (Figure 6, lower plots).

5. SPIN-POLARIZED TUNNELING THROUGH COPC

5.1. Introductory Remarks. Paramagnetic porphyrin and phthalocyanine (Pc) molecules, comprising 3d transition metal atoms, which are widely used in the manufacturing of light-emitting diodes and organic field-effect transistors, have recently attracted attention also in the spintronics community. They serve as prototype model systems where the arrangement of spins residing on molecules is attempted to be externally controlled by exchange coupling to the ferromagnetic substrates. For example, it has been revealed in the XMCD (X-ray circular magnetic dichroism) measurements of Wende et al.[8] that spins localized on Fe atoms of the prophyrin molecules deposited on Ni and Co films are arranged ferromagnetically (either out- or in-plane) vs the magnetization of the underlying substrate.

In this section, we would like to apply our computational machinery to study another prototype system, which is a paramagnetic (S = 1/2) CoPc molecule deposited on a Co nanoisland and probed, in the tunneling regime, by a Co-coated tip of the spin-polarized STM (see Figure 7a,b). Within the typical experimental setups,[11,12] Co islands exhibit spontaneous out-of-plane magnetization, which is aligned either (roughly) parallel (P) or antiparallel (AP) to the out-of-plane magnetization of the STM tip. By placing the tip above the CoPc molecules decorating Co nanoislands, bias dependent differential conductances $g(V) = dI/dV$ have been recorded by Iacovita et al.[11] Intriguingly, an asymmetry of the conductances, $(g_P - g_{AP})/(g_P + g_{AP})$, has been found to change a sign twice when probing energies down to −1 eV below the Fermi level. An origin of this observation remained almost unexplained. Furthermore, except for modeling the electron transport response, we consider this system to be challenging to address theoretically because of two reasons: (i) first, conductance is in the tunneling regime, which is due to a weak overlap between electronic wave functions of the tip and of the molecule adsorbed on the surface; (ii) second, a free 1/2 spin of the formerly isolated CoPc is subject to exchange interaction with the substrate, where a situation is overcomplicated by the correlation effects and a partial charge transfer.

5.2. Electronic Structure of Free and Adsorbed CoPc. To model a CoPc tunneling junction, we first have performed geometry optimization for the CoPc adsorbed on the fcc (111) surface, represented by a cluster of 65 Cu atoms. As has been already emphasized, the use of Co(111) clusters for structure optimization with TURBOMOLE has been impaired by the large number of energetically almost degenerate spin multiplets. The gradient corrected approximation (GGA[42,43]) DFT-energy was amended by empirical Grimme corrections[75] to account for van der Waals dispersion forces between the molecule and the surface. Our analysis suggests that CoPc prefers the "bridge" position (see Figure 7a) with a binding energy of −8.85 eV, relative to the "hollow" site position (binding energy −8.75 eV) which is consistent with earlier findings.[11,76] Furthermore, for the optimal distance between the molecule and the surface we have obtained an estimate of 2.71 Å, again in relatively good agreement with values reported in the earlier studies.[10]

The atomic configuration of the "extended molecule" used to simulate the bottleneck of the CoPc based tunneling junction is shown in Figure 7b: CoPc is bound to the Co(111) cluster with 51 atoms, representing the Co surface, while the smaller cluster with 19 atoms models the fcc Co tip. The tip is placed 4.54 Å above the CoPc and is slightly shifted from the center of the molecule. We have followed an approach presented in detail in section 2 to compute electronic structure of the open system. The infinite reservoirs with spin-polarized electrons have been modeled by the local spin-dependent self-energies (eq 2),

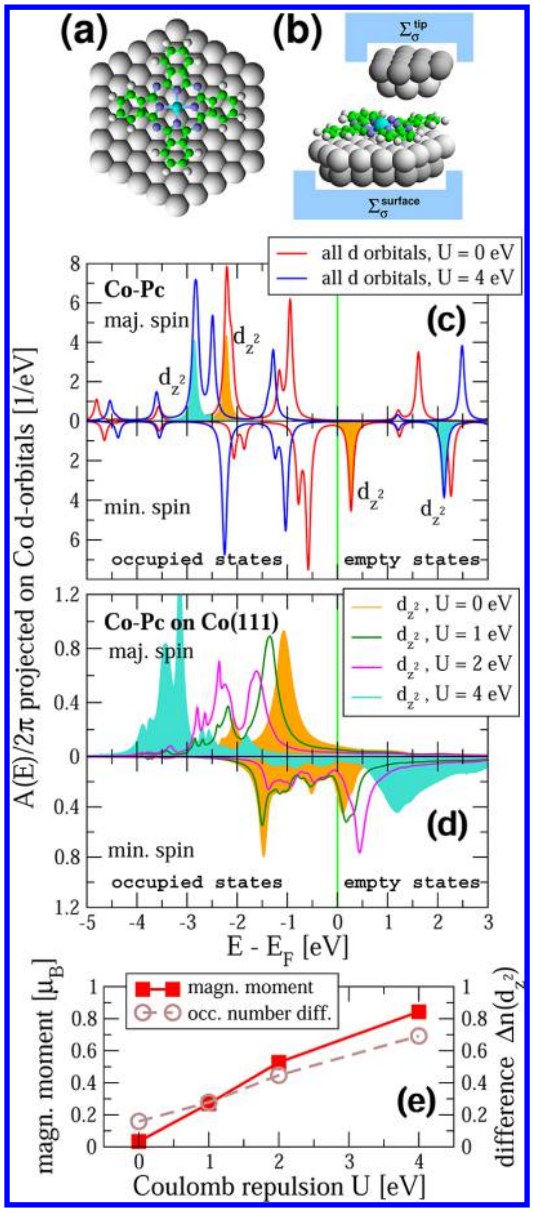

Figure 7. (a) CoPc molecule adsorbed in a "bridged" position on Co(111) surface. (b) Atomic configuration of the "extended molecule" used to evaluate electron tunneling characteristics across CoPc. (c) Kohn–Sham spectral function of a free CoPc molecule projected on Co d orbitals (artificial level broadening η = 0.05 eV is implied) computed within the GGA and GGA+U (=4.0 eV) functionals. (d) Spectral function of CoPc adsorbed on the Co(111) surface; spin dependent contributions associated with d_{z^2} orbitals at Co atom of CoPc are shown. (e) Residual magnetic moment at Co atom of CoPc as function of the Coulomb repulsion U, as well as a difference $\Delta n(d_{z^2}) = n^{\uparrow}(d_{z^2}) - n^{\downarrow}(d_{z^2})$ in the partial occupation numbers of up-spin and down-spin Co d_{z^2} states.

which are ascribed to the outermost boundaries of the simulation cluster (dark gray atoms at Figure 6b). A parameter $|\Delta_{ex}^{L/R}|$ = 1.6 eV has been used to account for the exchange splitting of the bulk Co d states.[47] We have ascertained that within our implementation of the NEGF method the electronic structure of the Co surface is properly reproduced: in particular, an exchange splitting 1.8 eV of the d states and a magnetic moment m(Co) ≈ 1.65 μ_B per a surface Co atom have been found, in agreement with previously reported calculations.[50] As before, freedom to choose a sign of $\Delta_{ex}^{L/R}$ independently for the "surface" and "STM-tip" clusters allows us to assemble two solutions with a parallel and antiparallel alignment of the electrodes' magnetizations.

We first restate some essential details of the electronic structure of the CoPc. A free molecule with D_{4h} symmetry is an open shell system with one unpaired electron populating the Co a_{1g} (d_{z^2}) out-of-plane orbital in the majority spin channel[77,78] (see Figure 7c). That also can be indirectly confirmed experimentally by analysis of the XMCD spectra.[79] Furthermore, the stability of this GGA type spin-DFT solution is confirmed, when on-site interaction U is switched on. Expected downward and upward shifts of the occupied and unoccupied electronic states are seen in the spectral function shown in Figure 7c.

Even though Co surface atoms have a mean magnetic moment of 1.65 μ_B, somewhat unexpected prediction of the spin-GGA functional is that the magnetic moment of the Co atom within the Pc molecule adsorbed on the surface remains almost quenched (Figure 7e). Our analysis reveals that this "quenched" moment arises because spectral weights associated with up- and down-spin d_{z^2} states are broadened by few electron volts, with a formerly unoccupied minority spin state being centered below the Fermi level (Figure 7d). A partial transfer of charge to the minority d_{z^2} state is compensated by a leakage of charge from other molecular orbitals hybridized with the surface. Similar results have been seen in the calculations involving FePc on magnetic Fe films.[10]

We would like to stress here that the above picture may be an artifact of the GGA functional. As visible from data presented in Figure 7d, when a self-interaction is corrected by including the Hubbard U term, the minority and majority d_{z^2} projected spectral functions develop into more localized resonances dressed by sub-bands but centered primary either below or above the Fermi energy. The expected value of the local magnetic moment at the Co atom within Pc correlates with the difference $\Delta n(d_{z^2}) = n^{\uparrow}(d_{z^2}) - n^{\downarrow}(d_{z^2})$ of partial occupations of the d_{z^2} states. The magnetic moment, ferromagnetically aligned to the surface magnetization, reappears and at large U = 4 eV reaches a value of 0.8 μ_B. A robust experimental verification of these results is challenging. However, we mention that recent XMCD measurements of the CoPc molecules adsorbed on Fe films[80] show signatures of local magnetic moments at Co atoms of Pc.

5.3. Electron Tunneling Characteristics. In Figure 8, we summarize results of our simulations of electron tunneling characteristics across CoPc. We first consider a transmission function decomposed in contributions due to majority and minority spins, shown in Figure 8a (here, we assume parallel alignment of magnetic moments in the tip and in the surface). In agreement with expectations of Tersoff–Hamann model,[81] we observe that around the Fermi level (E_F) the tunneling current is dominated by minority spin electrons, while the corresponding majority spin contributions are shifted ∼2.0 eV below the E_F, reflecting the spin-polarized band structure of the Co surface. Note also that the exponential-like increase of the tunneling transmission with increasing energy E of the electron, seen in our simulations, correctly reflects the modified height of the energy-dependent tunneling barrier ($\propto(|E|)^{1/2}$).

In Figures 8b–d, we present results of calculations highlighting the tunneling magnetoresistance effect across the CoPc. Shown transmission functions are computed assuming parallel (P) and antiparallel (AP) aligned magnetizations of the

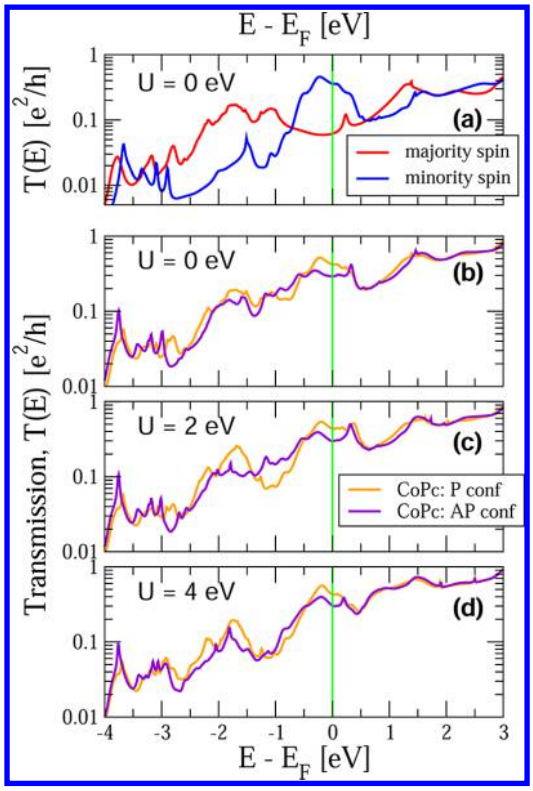

Figure 8. (a) Spin-resolved transmission functions across a CoPc tunnel junction with a parallel alignment of magnetizations in Co electrodes. (b–d) Energy dependent transmission functions across CoPc junctions with parallel (P) and antiparallel (AP) aligned magnetizations in Co electrodes. Calculations have been performed using a GGA exchange-correlation functional (plots a and b), and GGA+U with U = 2 eV (plot c) and 4 eV (plot d), respectively.

two Co electrodes. We summarize our observations. First, Coulomb repulsion U, which in essence modifies positions of the d states associated with a (central) Co atom of the molecule, only moderately affects the shape of the tunneling transmission curves: that is because d like orbitals of the central Co atom decay quite fast in the vacuum region and therefore are weakly coupled to the STM tip, they give only a minor contribution to the tunneling current. Second, the asymmetry of the tunneling probability, $[T_P(E) - T_{AP}(E)]/[T_P(E) + T_{AP}(E)]$, changes a sign twice, when scanning energies below E_F (down to −2 eV), so that our simulations qualitatively resemble the experimental observations of Iacovita et al.[11] At the Fermi level, the asymmetry of conductance, $(g_P - g_{AP})/(g_P + g_{AP})$, is on the order of ∼0.2, also similar to experimental observation (∼0.1). In spite of only qualitative agreement between theory and experiment, we note that our results illustrate a nontrivial impact of the hybridization between the CoPc and the surface: for example, a simple picture of tunneling across the Co/vacuum/Co barrier (assuming a free electron model with different Fermi momenta $k_F^{\uparrow,\downarrow}$ for majority and minority spin electrons[82]) predicts $g_P > g_{AP}$.

6. SUMMARY AND OUTLOOK

To summarize, we have presented an implementation of the DFT-based real-space version of the nonequilibrium Green's function formalism, where the emphasis has been put on the electron transport across molecules carrying spins and coupled to magnetic electrodes. We have implemented the method into original computer code AITRANSS, which is interfaced to the standard quantum chemistry package. We have demonstrated applications based on the implementation of DFT with Gaussian basis sets as provided by TURBOMOLE.[36] However, interfaces to other codes with local basis sets, e.g., FHI-aims,[39] are possible.

A particular distinction of our approach, underlying its efficiency, is the usage of the parametrized model self-energies that makes possible analytical evaluation of the spectral integral for the density matrix. The self-energies account both for the exchange splitting of electronic levels in the reservoirs as well as for a finite lifetime of excitations initially localized on the molecule and can be viewed as adsorbing (spin-dependent) boundary conditions[32,46] for the Kohn–Sham wave functions. We have shown that when a trial density matrix is iterated subject to such spin-dependent boundary conditions, a variety of (collinear) spin-ordered solutions within the molecular junction can be achieved in a controlled way. Depending on the imposed boundary conditions, each solution properly describes a relative alignment of magnetizations in the electrodes, as well as a mutual orientation of magnetic moments localized at open shell 3d atoms of the molecule. Thus, effects arising from the interplay between magnetism and quantum transport at atomic scale can be studied.

As an example, we have presented an analysis of the magnetoresistance effect (MR) in nanoscale systems with different conduction regimes: this includes Ni atomic scale contacts and vanadium-benzene sandwich clusters with metallic conductivity, as well as tunneling through Co-phthalocyanines in the STM geometry. Furthermore, our approach has already proven its efficiency in application to recent spin-polarized STM-based transport experiments[12,13] through hydrogen-phthalocyanine molecules.

We have also discussed an impact of correlation effects on the electron transport characteristics within the simplest DFT +U approach. At this point, we note that a recent implementation[83] of the quasiparticle GW method into TURBOMOLE opens a possibility for a more rigorous analysis in the future. Furthermore, a generalization of the transport formalism to the two-component spinor formulation is envisaged that will allow one to take effects of spin–orbit coupling and noncollinear spin-ordering into consideration.

APPENDIX A. EVALUATION OF THE SPECTRAL INTEGRAL FOR THE DENSITY MATRIX

Within the approximation of energy-independent self-energy, evaluation of the spectral integral in eq 3 can be performed analytically[31] using the eigenstate representation of the operator $(H^\sigma + \Sigma_L^\sigma + \Sigma_R^\sigma)$. Explicit expressions, implemented in our computer code, are listed below. In the following, we skip the obvious dependence of matrices on the spin index σ.

Let Z_p be the complex-valued eigenvalues, and columns of matrix B be the corresponding eigenvectors defined as

$$(H + \Sigma_L + \Sigma_R)B = BZ \tag{4}$$

where $Z = \mathrm{diag}\{Z_p\}$. Also, $G(E)B = B(E - Z)^{-1}$. Assuming a zero temperature limit, the spectral integral (eq 3) reads as

dx.doi.org/10.1021/ct4000263 | J. Chem. Theory Comput. 2013, 9, 2801–2815

$$D = \sum_{\alpha=\mathrm{L,R}} D_\alpha = \sum_{\alpha=\mathrm{L,R}} \int_{-\infty}^{\mu_\alpha} \frac{\mathrm{d}E}{2\pi} G(E)\Gamma_\alpha G^\dagger(E) = \sum_{\alpha=\mathrm{L,R}} BJ^\alpha B^\dagger \quad (5)$$

where $J^\alpha_{pp'} = [B^{-1}\Gamma_\alpha(B^\dagger)^{-1}]_{pp'}F_{pp'}(\mu_\alpha)$, with

$$F_{pp'}(\mu) = \int_{-\infty}^{\mu} \frac{\mathrm{d}E}{2\pi} \frac{1}{(E - Z_p)(E - Z_{p'})} \quad (6)$$

Let $Z_p = \omega_p - i\eta_p$ and $\varepsilon_p = \mu - \omega_p$. The above integrals are explicitly evaluated as

$$F_{pp'}(\mu) = \frac{1}{2\pi} \frac{1}{(\varepsilon_p - \varepsilon_{p'}) - i(\eta_p - \eta_{p'})} \times \left[-2\pi i + \frac{1}{2}\log\left(\frac{\varepsilon_p^2 + \eta_p^2}{\varepsilon_{p'}^2 + \eta_{p'}^2}\right) + i\arctan\frac{\eta_p}{\varepsilon_p} + i\arctan\frac{\eta_{p'}}{\varepsilon_{p'}} \right] \quad (7)$$

Note, that since the density operator is Hermitian ($D^\dagger = D$), and Gaussian basis functions are real, the charge density $n(\mathbf{x}) = \langle \mathbf{x}|D|\mathbf{x}\rangle = \Sigma_{\mu\mu'\nu\nu'}\varphi_\mu(\mathbf{x})\ S^{-1/2}_{\mu\mu'}D_{\mu'\nu'}\ S^{-1/2}_{\nu'\nu}\varphi_\nu(\mathbf{x})$ is a real quantity.

APPENDIX B. ELECTRON TRANSPORT THROUGH BENZENE-DITHIOL

In this appendix, we present a representative example illustrating a simulation of transmission curves $T(E)$ across a benzene-dithiol (BDT) molecule attached to gold electrodes. A bottleneck of the single molecule junction is modeled by "extended molecule" ($\mathcal{M}$) as shown in Figure 9a–d, where metallic Au leads are represented by two pyramidal fcc (001) clusters. The amount of atoms in the clusters is gradually increased from 15 (junction a), over 19 (junction b) and 29 (junction c), and up to 41 (junction d). Calculations have been performed using PBE exchange correlation functional[69] and the def-SVP basis set (of split-valence plus polarization quality) from the TURBOMOLE library.[44,45,84] Au atoms have been treated using effective core potentials,[85] with 19 valence and 60 core electrons.

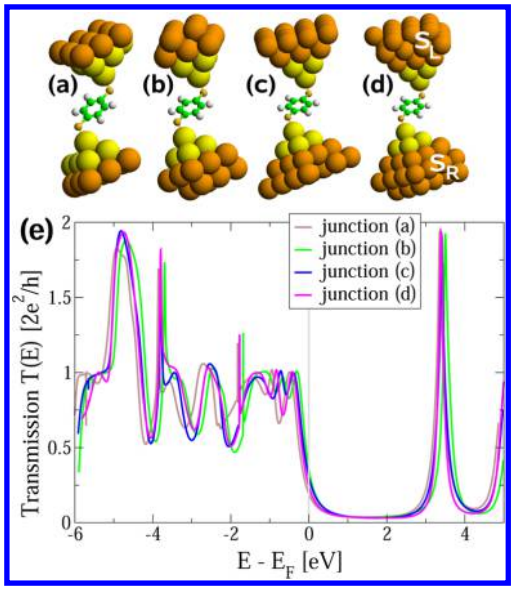

Figure 9. (a–d) Atomic structures used to simulate electron transport through a benzenedithiol molecule and (e) corresponding transmission curves.

The self-energies $\Sigma_{\mathrm{L/R}}$ have been approximated by the energy independent, local "leakage" function: $\Sigma_{\mathrm{L/R}}(\mathbf{x},\mathbf{x}') = \lambda(\mathbf{x})[\delta\varepsilon - i\eta]\delta(\mathbf{x} - \mathbf{x}')$, which has nonzero (diagonal) matrix elements only within the marked (dark yellow) regions $\mathcal{S}_\mathrm{L}$ and $\mathcal{S}_\mathrm{R}$ of the Au clusters as shown in Figure 9a–d. On the basis of earlier estimates,[32] a model parameter η equals 2.72 eV. A dimensionless function $\lambda(\mathbf{x})$ accounts for a gradual switching of perturbation: $\lambda(\mathbf{x}) = 1.0$ if $\mathbf{x}$ is within the outermost "surface" atomic plane of the Au cluster, $\lambda(\mathbf{x}) = 0.5$ if $\mathbf{x}$ is within the "surface-1" atomic layer and within $\mathcal{S}_{\mathrm{L/R}}$, and $\lambda(\mathbf{x}) = 0.25$ if $\mathbf{x}$ is within the "surface-2" atomic layer and within $\mathcal{S}_{\mathrm{L/R}}$. The value of the Fermi energy has been taken as an average of energies of the HOMO and LUMO levels of the "extended molecule," $E_F \simeq (\varepsilon_H^{\mathcal{M}} + \varepsilon_L^{\mathcal{M}})/2$. The energy shift $\delta\varepsilon$ parametrizing the self-energy has been adjusted to satisfy a charge neutrality condition within the "extended molecule" $\mathcal{M}$ as follows from the density matrix of the open system defined in eq 3.

Transmission functions $T(E)$ across the BDT, computed using different models for electrodes, are shown in Figure 9e. We mention the following essential points: (a) when adsorbing boundaries are characterized by strong damping η, which is significantly larger that mean level spacing in the "extended molecule" $\mathcal{M}$, $T(E)$ shows (as it should) molecular resonances but not "cavity modes". (b) Widths of resonances are almost insensitive to the precise amount of Au atoms used to simulate the electrodes. (c) Exact positions of resonances fluctuate up to ~100 meV, which is a manifestation of the finite size effects; when larger simulation clusters are used, only minor differences are observed between computed transmission functions. In this regard, one should keep in mind that another source of errors in the prediction of the positions, and also widths, of molecular resonances is a missing derivative discontinuity inherent to the approximate (local or quasi-local) xc functionals. Thus, "standard" DFT based transmission curves provide us with qualitative information on the electron transport across organic molecules. Note, that recent works on lattice models[25−28] show evidence that the use of the exact xc-functional (when available) can give, under certain conditions, an almost precise description of the conductance through an interacting quantum dot.

APPENDIX C. IMPLEMENTATION OF DFT+*U* METHOD

In this appendix, we outline essential details of the implementation of the DFT+*U* approach. For the given molecular junction, we usually select few low-coordinated atoms, $N_\mathcal{C}$ with open d shells where electron correlations will be treated on the Hartree–Fock level. For example, in the case of Ni–V_2Bz_3–Ni junction, considered in section 4, these are the two V atoms of the V_2Bz_3 cluster coupled to Ni electrodes, but not Ni atoms. In the example presented in section 5, this is a single Co atom of the CoPc molecule deposited on the Co nanoisland, but not Co atoms of the surface (Figure 7a,b).

We follow a formulation of the method presented by Dudarev et al.,[86] where corrections to a single particle potential

are given in terms of density matrix of d electrons. For that, one needs to define a "correlated subspace" C, spanned by localized orbitals centered at selected atoms. To this end, we consider Gaussian type orbitals (GTOs) inherent to TURBOMOLE, where each 3d transition metal atom is described by a set of the contracted orbitals (CGTOs).[44] For example, in the case of SVP basis, this set is of the type [5s3p2d]/{63311|531|41}. Here [k, l, m] denotes the number of CGTOs of s, p, and d character, and $\{s_1s_2...|p_1p_2...|d_1d_2...\}$ denotes the contraction pattern.[44] In particular, a 3d shell is represented by two types of basis functions. The first one, a superposition of four Gaussians, describes an atomic d function, while the second one is a single diffuse Gaussian orbital with a small exponent. In a similar way, in the case of triple-ζ quality basis sets,[87] two out of the three different d type CGTOs are diffuse. A natural assumption to define the correlated subspace C is to consider only d atomic-like contracted orbitals $|\alpha\rangle$ (actually, five per selected atom), but not the diffuse d orbitals. Thus, a dimension of the subspace C (per spin channel σ) is $5N_c$.

Next, let $\Omega_{\alpha\beta} = \langle\alpha|\beta\rangle$ be the overlap integrals, and $|\tilde{\alpha}\rangle = \sum_{\alpha'\in C}|\alpha'\rangle\Omega^{-1/2}_{\alpha'\alpha}$ be the orthogonal basis in C. Consider the KS Hamiltonian (eq 1) and the density matrix (eq 3) projected on C: $H^d = \Sigma_\sigma H^{d,\sigma}$ and $\rho^d = \Sigma_\sigma \rho^{d,\sigma}$, where

$$H^{d,\sigma} = \sum_{\alpha\beta\in C}|\tilde{\alpha}\rangle\langle\tilde{\alpha}|H^\sigma|\tilde{\beta}\rangle\langle\tilde{\beta}| = \sum_{\alpha\beta\in C}|\tilde{\alpha}\rangle H^{d,\sigma}_{\alpha\beta}\langle\tilde{\beta}| \tag{8}$$

and

$$\rho^{d,\sigma} = \sum_{\alpha\beta\in C}|\tilde{\alpha}\rangle\langle\tilde{\alpha}|D^\sigma|\tilde{\beta}\rangle\langle\tilde{\beta}| = \sum_{\alpha\beta\in C}|\tilde{\alpha}\rangle D^{d,\sigma}_{\alpha\beta}\langle\tilde{\beta}| \tag{9}$$

with the Hamiltonian matrix elements given by

$$H^{d,\sigma}_{\alpha\beta} = \sum_{\alpha'\beta'\in C,\mu\nu}\Omega^{-1/2}_{\alpha\alpha'}S^{1/2}_{\alpha'\mu}H^\sigma_{\mu\nu}S^{1/2}_{\nu\beta'}\Omega^{-1/2}_{\beta'\beta} \tag{10}$$

and the density matrix elements expressed as

$$\rho^{d,\sigma}_{\alpha\beta} = \sum_{\alpha'\beta'\in C,\mu\nu}\Omega^{-1/2}_{\alpha\alpha'}S^{1/2}_{\alpha'\mu}D^\sigma_{\mu\nu}S^{1/2}_{\nu\beta'}\Omega^{-1/2}_{\beta'\beta} \tag{11}$$

The KS Hamiltonian projected on C (eq 8) can be diagonalized, $\sum_{\alpha\beta\in C}U^{\sigma\dagger}_{m\alpha}H^{d,\sigma}_{\alpha\beta}U^\sigma_{\beta m'} = \varepsilon_m\delta_{mm'}$, where ε_m are eigenvalues, and $|m\rangle = \sum_{\alpha\in C}|\tilde{\alpha}\rangle U_{\alpha m}$ are corresponding eigenvectors. Further, let $\rho^{d,\sigma}_{mm'} = \sum_{\alpha\beta\in C}U^{\sigma\dagger}_{m\alpha}\rho^{d,\sigma}_{\alpha\beta}U^\sigma_{\beta m'}$ be elements of the d electron density matrix in the basis $|m\rangle$. In the DFT+U approach, the Hamiltonian of d electrons is modified *ad hoc* by adding the term defined through the elements of the density matrix:[86]

$$\begin{aligned}\delta H^{d,\sigma} &= \sum_{mm'\in C}|m\rangle\delta H^{d,\sigma}_{mm'}\langle m'| \\ &= \frac{U}{2}\sum_{mm'\in C}|m\rangle(\delta_{mm'} - 2\rho^{d,\sigma}_{m'm})\langle m'|\end{aligned} \tag{12}$$

Here, U has a meaning of the spherically averaged matrix elements of the screened Coulomb interaction, including direct and exchange terms. In case the density matrix is diagonal in the $|m\rangle$ basis, $\rho^{d,\sigma}_{mm'} = n_m\delta_{mm'}$ with n_m being occupation numbers; energies ε_m of levels associated with d electrons are shifted by $\delta\varepsilon_m = (U/2)(1 - 2n_m)$. In particular, the energy of the fully occupied state is shifted down by $-(U/2)$, while the empty level is shifted upward by $+(U/2)$.

The correction term $\delta H^{d,\sigma}$ to the Hamiltonian (eq 12) defined on C should be mapped back onto the Hilbert space of the entire system:

$$\delta H^{d,\sigma} = \sum_{\mu\nu}|\tilde{\mu}\rangle\delta H^\sigma_{\mu\nu}\langle\tilde{\nu}| \tag{13}$$

where

$$\delta H^\sigma_{\mu\nu} = \sum_{mm'\in C}\langle\tilde{\mu}|m\rangle\delta H^{d,\sigma}_{mm'}\langle m'|\tilde{\nu}\rangle \tag{14}$$

An explicit expression for $\delta H^\sigma_{\mu\nu}$ is

$$\begin{aligned}\delta H^\sigma_{\mu\nu} = &\sum_{\alpha\alpha' mm'\beta\beta'\in C}S^{1/2}_{\mu\alpha}\Omega^{-1/2}_{\alpha\alpha'}U^\sigma_{\alpha' m}\times \\ &\times\delta H^{d,\sigma}_{mm'}U^{\sigma\dagger}_{m'\beta'}\Omega^{-1/2}_{\beta'\beta}S^{1/2}_{\beta\nu}\end{aligned} \tag{15}$$

Finally, the self-consistent DFT+U solution reached when the density matrix (eq 3) is iterated assuming the Green's function $G^\sigma_{\mu\nu}(E)$ is defined via the Hamiltonian, $H^\sigma_{\mu\nu} + \delta H^\sigma_{\mu\nu}$, with corrections included.

AUTHOR INFORMATION

Corresponding Author

*E-mail: alexej.bagrets@kit.edu.

Notes

The authors declare no competing financial interest.

ACKNOWLEDGMENTS

The author expresses his gratitude to F. Evers, A. Arnold, F. Weigend, V. Meded, W. Wulfhekel, M. J. van Setten, V. Blum, and K. Fink for fruitful discussions. Financial support by the German Research Foundation (DFG grant BA-4265) is gratefully acknowledged.

REFERENCES

(1) Baibich, M. N.; Broto, J. M.; Fert, A.; Van Dau, F. N.; Petroff, F.; Etienne, P.; Creuzet, G.; Friederich, A.; Chazelas, J. *Phys. Rev. Lett.* **1988**, *61*, 2472−2475.

(2) Binasch, G.; Grünberg, P.; Saurenbach, F.; Zinn, W. *Phys. Rev. B* **1989**, *39*, 4828−4830.

(3) Schlegel, C.; van Slageren, J.; Manoli, M.; Brechin, E. K.; Dressel, M. *Phys. Rev. Lett.* **2008**, *101*, 147203.

(4) Liljeroth, P.; Repp, J.; Gerhard, M. *Science* **2007**, *317*, 1203−1206.

(5) Iancu, V.; Deshpande, A.; Hla, S.-W. *Nano Lett.* **2006**, *6*, 820−823.

(6) Iancu, V.; Deshpande, A.; Hla, S.-W. *Phys. Rev. Lett.* **2006**, *97*, 266603.

(7) Bernien, M.; Miguel, J.; Weis, C.; Ali, M. E.; Kurde, J.; Krumme, B.; Panchmatia, P. M.; Sanyal, B.; Piantek, M.; Srivastava, P.; Baberschke, K.; Oppeneer, P. M.; Eriksson, O.; Kuch, W.; Wende, H. *Phys. Rev. Lett.* **2009**, *102*, 047202.

(8) Wende, H.; Bernien, M.; Luo, J.; Sorg, C.; Ponpandian, N.; Kurde, J.; Miguel, J.; Piantek, M.; Xu, X.; Eckhold, P.; Kuch, W.; Baberschke, K.; Panchmatia, P. M.; Sanyal, B.; Oppeneer, P. M.; Eriksson, O. *Nat. Mater.* **2007**, *6*, 516−520.

(9) Atodiresei, N.; Brede, J.; Lazić, P.; Caciuc, V.; Hoffmann, G.; Wiesendanger, R.; Blügel, S. *Phys. Rev. Lett.* **2010**, *105*, 066601.

(10) Brede, J.; Atodiresei, N.; Kuck, S.; Lazić, P.; Caciuc, V.; Morikawa, Y.; Hoffmann, G.; Blügel, S.; Wiesendanger, R. *Phys. Rev. Lett.* **2010**, *105*, 047204.

(11) Iacovita, C.; Rastei, M. V.; Heinrich, B. W.; Brumme, T.; Kortus, J.; Limot, L.; Bucher, J. P. *Phys. Rev. Lett.* **2008**, *101*, 116602.

(12) Schmaus, S.; Bagrets, A.; Nahas, Y.; Yamada, T. K.; Bork, A.; Bowen, M.; Beaurepaire, E.; Evers, F.; Wulfhekel, W. *Nat. Nanotechnol.* **2011**, *6*, 185−189.
(13) Bagrets, A.; Schmaus, S.; Jaafar, A.; Kramczynski, D.; Yamada, T. K.; Alouani, M.; Wulfhekel, W.; Evers, F. *Nano Lett.* **2012**, *12*, 5131−5136.
(14) Brandbyge, M.; Mozos, J.-L.; Ordejón, P.; Taylor, J.; Stokbro, K. *Phys. Rev. B* **2002**, *65*, 165401.
(15) Pecchia, A.; Di Carlo, A. *Rep. Prog. Phys.* **2004**, *67*, 1497.
(16) Rocha, A. R.; García-Suárez, V. M.; Bailey, S.; Lambert, C.; Ferrer, J.; Sanvito, S. *Phys. Rev. B* **2006**, *73*, 085414.
(17) Verzijl, C. J. O.; Thijssen, J. M. *J. Phys. Chem. C* **2012**, *116*, 24393−Ű24412.
(18) Evers, F.; Kieron, B. In *Nano and Molecular Electronics Handbook*; Lyshevski, S., Ed.; CRC Press: Boca Raton, FL, 2007; pp 24.
(19) Li, C.; Pobelov, I.; Wandlowski, T.; Bagrets, A.; Arnold, A.; Evers, F. *J. Am. Chem. Soc.* **2008**, *130*, 318−326.
(20) Ruben, M.; Landa, A.; Lörtscher, E.; Riel, H.; Mayor, M.; Görls, H.; Weber, H. B.; Arnold, A.; Evers, F. *Small* **2008**, *4*, 2229.
(21) Quek, S. Y.; Kamenetska, M.; Steigerwald, M. L.; Choi, H. J.; Louie, S. G.; Hybertsen, M. S.; Neaton, J. B.; Venkataraman, L. *Nat. Nanotechnol.* **2009**, *4*, 230−234.
(22) Meded, V.; Bagrets, A.; Arnold, A.; Evers, F. *Small* **2009**, *5*, 2218−2223.
(23) Schull, G.; Frederiksen, T.; Brandbyge, M.; Berndt, R. *Phys. Rev. Lett.* **2009**, *103*, 206803.
(24) Guédon, C. M.; Valkenier, H.; Markussen, T.; Thygesen, K. S.; Hummelen, J. C.; van der Molen, S. J. *Nat. Nanotechnol.* **2012**, *7*, 305−309.
(25) Schmitteckert, P.; Evers, F. *Phys. Rev. Lett.* **2008**, *100*, 086401.
(26) Tröster, P.; Schmitteckert, P.; Evers, F. *Phys. Rev. B* **2012**, *85*, 115409.
(27) Stefanucci, G.; Kurth, S. *Phys. Rev. Lett.* **2011**, *107*, 216401.
(28) Bergfield, J. P.; Liu, Z.-F.; Burke, K.; Stafford, C. A. *Phys. Rev. Lett.* **2012**, *108*, 066801.
(29) Turek, I.; Drchal, V.; Kudrnovský, J.; Šob, M.; Weinberger, P. *Electronic Structure of Disordered Alloys, Surfaces and Interfaces*; Kluwer Academic: Boston, 1997.
(30) Jacob, D.; Palacios, J. J. *J. Chem. Phys.* **2011**, *134*, 044118.
(31) Arnold, A.; Evers, F.; Weigend, F. *J. Chem. Phys.* **2007**, *126*, 174101.
(32) Evers, F.; Arnold, A. In *CFN Lectures on Functional Nanostructures - Vol. 2: Nanoelectronics*, Lecture Notes in Physics, Vol. *820*; Vojta, M., Röthig, C., Schön, G., Eds.; Springer-Verlag: Berlin, 2011; pp 27−53.
(33) Baadji, N.; Sanvito, S. *Phys. Rev. Lett.* **2012**, *108*, 217201.
(34) Hardrat, B.; Wang, N.-P.; Freimuth, F.; Mokrousov, Y.; Heinze, S. *Phys. Rev. B* **2012**, *85*, 245412.
(35) Hardrat, B.; Freimuth, F.; Heinze, S.; Mokrousov, Y. *Phys. Rev. B* **2012**, *86*, 165449.
(36) Ahlrichs, R.; et al. *TURBOMOLE V5.10*; TURBOMOLE GmbH: Karlsruhe, Germany, 2008. Available from www.turbomole.com.
(37) Wilhelm, J.; Walz, M.; Stendel, M.; Bagrets, A.; Evers, F. *Phys. Chem. Chem. Phys.* **2013**, *15*, 6684−6690.
(38) AITRANSS package is available upon request by contacting the author via e-mail: alexej.bagrets@kit.edu.
(39) Blum, V.; Gehrke, R.; Hanke, F.; Havu, P.; Havu, V.; Ren, X.; Reuter, K.; Scheffler, M. *Comput. Phys. Commun.* **2009**, *180*, 2175−2196.
(40) Agraït, N.; Levy-Yeyati, A.; van Ruitenbeek, J. M. *Phys. Rep.* **2003**, *377*, 81−279.
(41) Park, H.; Lim, A. K. L.; Alivisatos, A. P.; Park, J.; McEuen, P. L. *Appl. Phys. Lett.* **1994**, *75*, 301−303.
(42) Becke, A. D. *Phys. Rev. A* **1988**, *38*, 3098−3100.
(43) Perdew, J. P. *Phys. Rev. B* **1986**, *33*, 8822−8824.
(44) Schäfer, A.; Horn, H.; R., A. *J. Chem. Phys.* **1992**, *97*, 2571.
(45) Eichkorn, K.; Treutler, O.; Öhm, H.; Häser, M.; Ahlrichs, R. *Chem. Phys. Lett.* **1995**, *242*, 652.
(46) Goyer, F.; Ernzerhof, M.; Zhuang, M. *J. Chem. Phys.* **2007**, *126*, 144104.
(47) Moruzzi, V. L.; Janak, J. F.; Williams, A. R. *Calculated Electronic Properties of Metals*; Pergamon Press: New York, 1978.
(48) Baker, B. G.; Johnson, B. B.; Maire, G. L. C. *Surf. Sci.* **1971**, *24*, 572−586.
(49) Burton, J. D.; Sabirianov, R. F.; Jaswal, S. S.; Tsymbal, E. Y.; Mryasov, O. N. *Phys. Rev. Lett.* **2006**, *97*, 077204.
(50) Bagrets, A.; Papanikolaou, N.; Mertig, I. *Phys. Rev. B* **2007**, *75*, 235448.
(51) Smogunov, A.; Dal Corso, A.; Tosatti, E. *Phys. Rev. B* **2006**, *73*, 075418.
(52) Bagrets, A.; Papanikolaou, N.; Mertig, I. *Phys. Rev. B* **2004**, *70*, 064410.
(53) Jacob, D.; Fernández-Rossier, J.; Palacios, J. J. *Phys. Rev. B* **2005**, *71*, 220403.
(54) Calvo, M. R.; Fernández-Rossier, J.; Palacios, J. J.; Jacob, D.; Natelson, D.; Untiedt, C. *Nature* **2009**, *458*, 1150−1153.
(55) Lucignano, P.; Mazzarello, R.; Smogunov, A.; Fabrizio, M.; Tosatti, E. *Nat. Mater.* **2009**, *8*, 563−567.
(56) Czerner, M.; Yavorsky, B. Y.; Mertig, I. *Phys. Rev. B* **2008**, *77*, 104411.
(57) Luzon, J.; Bernot, K.; Hewitt, I. J.; Anson, C. E.; Powell, A. K.; Sessoli, R. *Phys. Rev. Lett.* **2008**, *100*, 247205.
(58) Maslyuk, V. V.; Mertig, I.; Farberovich, O. V.; Tarantul, A.; Tsukerblat, B. *Eur. J. Inorg. Chem.* **2013**, 1897−1902.
(59) Peralta, J. E.; Scuseria, G. E.; Frisch, M. J. *Phys. Rev. B* **2007**, *75*, 125119.
(60) Armbruster, M. K.; Weigend, F.; van Wüllen, C.; Klopper, W. *Phys. Chem. Chem. Phys.* **2008**, *10*, 1748−1756.
(61) Nagaoka, S.; Matsumoto, T.; Ikemoto, K.; Mitsui, M.; Nakajima, A. *J. Am. Chem. Soc.* **2007**, *129*, 1528−1529.
(62) Nagaoka, S.; Ikemoto, K.; Fujio, K.; Hiehata, K.; Sasahara, A.; Mitsui, M.; Onishi, H.; Nakajima, A. *Eur. Phys. J. D* **2009**, *52*, 103−106.
(63) Schwöbel, J.; Fu, Y.; Brede, J.; Dilullo, A.; Hoffmann, G.; Klyatskaya, S.; Ruben, M.; Wiesendanger, R. *Nat. Commun.* **2012**, *3*, 953.
(64) Lodi Rizzini, A.; Krull, C.; Balashov, T.; Kavich, J. J.; Mugarza, A.; Miedema, P. S.; Thakur, P. K.; Sessi, V.; Klyatskaya, S.; Ruben, M.; Stepanow, S.; Gambardella, P. *Phys. Rev. Lett.* **2011**, *107*, 177205.
(65) Mittendorfer, F.; Hafner, J. *Surf. Sci.* **2001**, *472*, 133.
(66) Maslyuk, V. V.; Bagrets, A.; Meded, V.; Arnold, A.; Evers, F.; Brandbyge, M.; Bredow, T.; Mertig, I. *Phys. Rev. Lett.* **2006**, *97*, 097201.
(67) Xiang, H.; Yang, J.; Hou, J. G.; Zhu, Q. *J. Am. Chem. Soc.* **2006**, *128*, 2310−2314.
(68) Mokrousov, Y.; Atodiresei, N.; Bihlmayer, G.; Heinze, S.; Blügel, S. *Nanotechnology* **2007**, *18*, 495402.
(69) Perdew, J. P.; Burke, K.; Ernzerhof, M. *Phys. Rev. Lett.* **1996**, *77*, 3865−3868.
(70) Evers, F.; Weigend, F.; Koentopp, M. *Phys. Rev. B* **2004**, *69*, 235411.
(71) Neaton, J. B.; Hybertsen, M. S.; Louie, S. G. *Phys. Rev. Lett.* **2006**, *97*, 216405.
(72) Thygesen, K. S.; Rubio, A. *Phys. Rev. Lett.* **2009**, *102*, 046802.
(73) Anisimov, V. I.; Aryasetiawan, F.; Lichtenstein, A. I. *J. Phys.: Condens. Matt.* **1997**, *9*, 767.
(74) Kümmel, S.; Kronik, L. *Rev. Mod. Phys.* **2008**, *80*, 3−60.
(75) Grimme, S. *J. Comput. Chem.* **2006**, *27*, 1787−1799.
(76) Heinrich, B. W.; Iacovita, C.; Brumme, T.; Choi, D.-J.; Limot, L.; Rastei, Mircea, V.; Hofer, W. A.; Kortus, J.; Bucher, J.-P. *J. Phys. Chem. Lett.* **2010**, *1*, 1517−1523.
(77) Marom, N.; Kronik, L. *Appl. Phys. A: Mater. Sci. Process.* **2009**, *95*, 159−163.
(78) Mugarza, A.; Robles, R.; Krull, C.; Korytár, R.; Lorente, N.; Gambardella, P. *Phys. Rev. B* **2012**, *85*, 155437.

(79) Stepanow, S.; Miedema, P. S.; Mugarza, A.; Ceballos, G.; Moras, P.; Cezar, J. C.; Carbone, C.; de Groot, F. M. F.; Gambardella, P. *Phys. Rev. B* **2011**, *83*, 220401.
(80) Annese, E.; Fujii, J.; Vobornik, I.; Panaccione, G.; Rossi, G. *Phys. Rev. B* **2011**, *84*, 174443.
(81) Tersoff, J.; Hamann, D. R. *Phys. Rev. B* **1985**, *31*, 805−813.
(82) Vedyayev, A.; Bagrets, D.; Bagrets, A.; Dieny, B. *Phys. Rev. B* **2001**, *63*, 064429.
(83) van Setten, M. J.; Weigend, F.; Evers, F. *J. Chem. Theory Comput.* **2013**, *9*, 232−246.
(84) Eichkorn, K.; Weigend, F.; Treutler, O.; Ahlrichs, R. *Theor. Chem. Acc.* **1997**, *97*, 119.
(85) Andrae, D.; Haeussermann, U.; Dolg, M.; Stoll, H.; Preuss, H. *Theor. Chem. Acc.* **1990**, *77*, 123−141.
(86) Dudarev, S. L.; Botton, G. A.; Savrasov, S. Y.; Humphreys, C. J.; Sutton, A. P. *Phys. Rev. B* **1998**, *57*, 1505−1509.
(87) Schäfer, A.; Huber, C.; Ahlrichs, R. *J. Chem. Phys.* **1994**, *100*, 5829.